Università degli Studi di Firenze

DOTTORATO DI RICERCA IN

Energetica e Tecnologie Industriali Innovative

XXV° Ciclo

COORDINATORE Prof. Maurizio De Lucia

On the study of hydrogen fueling in premixed gas turbine combustor chamber

Settore Scientifico Disciplinare IND/08-09

Anni 2010/2012

Dottorando:

Dott. Ing. Alessandro Cappelletti

_____

Tutor

Prof. Francesco Martelli

_____

To Cristina and my Parents

“A mind is like a parachute. It doesn't work if it is not open”

Frank Zappa

Index

Nomenclature

c	progress variable	[-]
D	outlet diameter	[m]
Da	Damkholer number	[-]
f	mixture fraction	[-]
k	turbulent kinetic energy	[m^2/s^2]
m	mass flow rate	[kg/s]
p	pressure	[Pa]
Pr	Prandtl number	[-]
Re	Reynolds number	[-]
Sc	Schmidt number	[-]
SF	segregation factor	[-]
STD	standard deviation	[-]
Sw	swirl number	[-]
t	time	[s]
T	temperature	[K]
u	velocity	[m/s]
CFD	Computational Fluid Dynamics	
DLN	Dry Low NOx	
HSI	High Swirl Injector	
IGCC	Integrated Gasification Combined Cycle	
LES	Large Eddy Simulation	
LSI	Low Swirl Injector	
NO_x	Ossidi di Azoto	
PDF	Probability Density Function	
RANS	Reynolds Averaged Navier Stokes	

RSM	Reynolds Stress Models
SST	Shear Stress Models
GT	Gas Turbine
URANS	Unsteady Reynolds Averaged Navier Stokes

Greek

α	air/fuel ratio	[-]
δ_{ij}	Kronecker delta	[-]
ε	turbulent dissipation	[W]
Σ	flame surface density	[1/m]
μ	dynamic viscosity	[kg/(m/s)]
ω	specific turbulent dissipation	[1/s]
ρ	density	[kg/m^3]
ϕ	equivalent ratio	[-]

Subscripts and Superscripts

b	burned
l	laminar
st	stochiometric
t	turbulent
u	unburned

Introduction

The energy demand and the environmental protection ask for the development of new and improved technologies for low emission power plants designed to be fired by fuels derived from coal gasification. This kind of plant will utilize advanced gas turbine based IGCC cycles. The use of hydrogen as syngas fuel in gas turbine combustors provides environmental benefits with respect to natural gas because negligible quantities of CO, UHC and PAH are released.

Also hydrogen could be used as a energy buffer for renewable energy power plants or for the utilization of waste from petrochemistry industry.

However, the use of hydrogen as fuel is nowadays limited to gas turbines equipped by diffusive-type combustors, where the pure hydrogen supply leads to NOx emissions three times higher than those of the natural gas firing. Methods for reducing pollutant emissions are borrowed from those used in diffusive gas turbine combustion chambers supplied by natural gas.

Advanced options to be explored are represented by catalytic and premixed combustion technologies. Although the latter represents a mature technology for reducing NOx emission in gas turbine supplied with conventional fuels, its application to hydrogen fired gas turbines is hampered by the high flame propagation velocity and by the wider air-fuel ignition range which lead to flashback and explosion risks.

Several experiences/studies on premixed hydrogen combustion for gas turbine combustors have been carried out during the last decade.

The objective of the work described below was to explore the potential of reducing NOx emission from hydrogen combustion by means of air-fuel premixing.

The work is characterized by the using of numerical simulation and experimental activities on a prototype premixer.

The first phase was the design of the prototype with the support of numerical simulation and after the unit was tested at atmospheric pressure condition.

The experimental activities investigated the influence of the fuel, the thermal input and equivalence ratio on the NOx emission, the flame shape and the flash back.

The result emphasized the difficulty of hydrogen fueling with low NOx emission but it wasn't able to show same important aspects on the flame and the NOx emission.

Another interesting aspect showed by the experimental result was that the numerical approach validated on methane fueled cases is insufficient for hydrogen cases.

The work was continued with a improvement on numerical procedure analyzing both unsteady and steady approaches .

Individuated a adequate procedure the investigation continued on the analyzing of NOx emission path and the flame shape.

From all obtained data it was possible to individuate a gas turbine class fitted to hydrogen fueling, in fact the work concludes with the analyzing on a hydrogen fueled MGT combustor chamber.

Chapter 1.

Hydrogen Combustion in Gas Turbine

1.1 Hydrogen proprieties

The aim of this work is the possibility analyzing of the hydrogen fueling for a gas turbine with low NOx emission. The current experience on premixing technology comes from the natural gas fueling, thus the knowledge of hydrogen proprieties is important for the retrofitting.

In the last decades the lean premixed combustion is the dominant technology in gas turbine field for its low NOx emission [1]

The main issue of premixed combustion is the limited operative range in fact there are three bounding phenomena: the blowout, the flashback and the autoignition.

The next paragraphs describe the influence of hydrogen on these phenomena.

1.2 Laminar flame speed

The laminar flame speed is the main element for all premixed flames because it defines the position of flame front also in the cases with turbulent flame as in a gas turbine. There are many analytic correlations between laminar and turbulent flame speed [2].

The flame speed is also an important parameter for the numerical simulation because it permits to check the solution's quality.

The literature shows many theoretic and experimental value of laminar flame speed for different temperature, pressure and equivalence ratio.

Shelil et al. [3] evaluated the laminar flame speed for CH4/H2 mixture in many operative conditions with a numerical approach.

In the case with a hydrogen concentration less than 30% the difference are limited, see Figure 1-1, but the increase of hydrogen content moves high minor speed to very higher values.

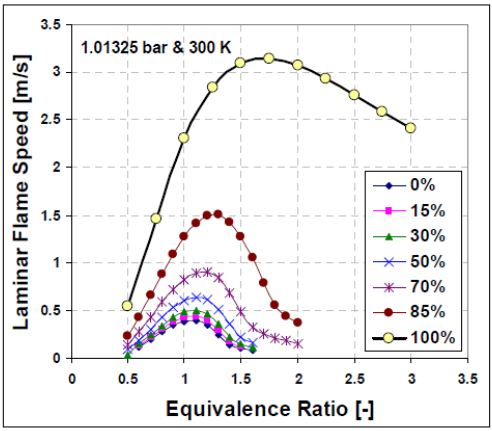

Figure 1-1: Laminar flame speed for CH4/H2 mixture in atmospheric condition and 300K temperature [3]

In the 100% hydrogen case, the maximal value of laminar flame speed is over 3 m/s for the equivalence value of 1,8 for the 100% methane the maximum is about 0,5 m/s.

The results of Shelil et al [3] are coherent with the experimental result of Kwon [4] and Rozenchan [5], see Figure 1-2.

Pareja et al. [6] collected many data of laminar flame speed in atmospheric condition, see Figure 1-7.

Kittagawa et al. [7] and Hu et al. [8] report the influence of pressure on laminar flame speed, see Figure 1-4 and Figure 1-5. Generally for equivalent ratio under 1 and over 2,5 the values decrease, absolute difference value is about 0,5 m/s.

Verhelst et al. [9] reports a high influence of temperature on the laminar flame speed for high pressure cases, see Figure 1-6.

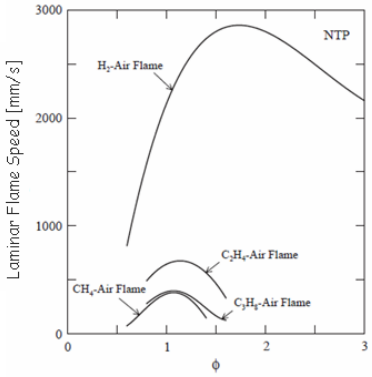

Figure 1-2: Experimental value of laminar flame speed for different mixture

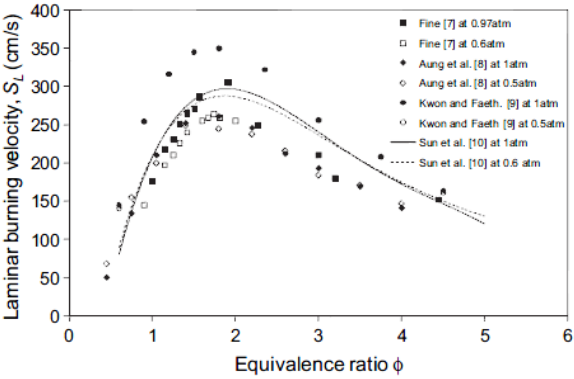

Figure 1-3: Laminar flame speed for H2/ Air mixture at atmospheric pressure and lower. Markers: experimental data; lines: numerical result.

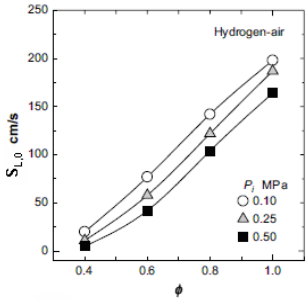

Figure 1-4: Laminar flame speed for H2/Air mixture for different pressure [7]

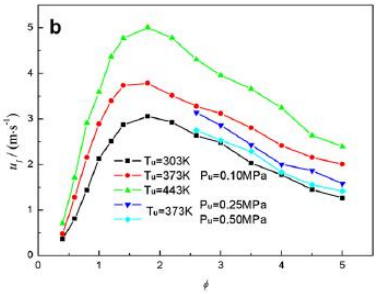

Figure 1-5: Laminar flame speed for H2/Air mixture for different pressure and temperature. [8]

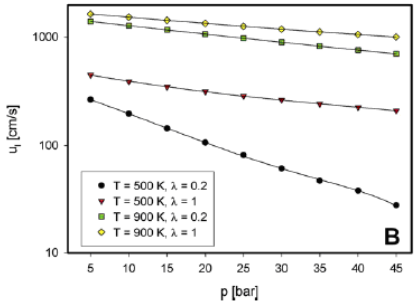

Figure 1-6: Laminar flame speed for H2/Air mixture for different pressure and temperature. [9]

1.3 Blowout and flashback

Many works on the flame stability and its propagation of lean CH4/Air premixed flames was produced in last decades [10].

The characterization of hydrogen flames isn't enough complete as for the methane ones. The first works were on the CH4/H2 mixture by Schefer et al. [11] but his intent was to improve the stability of methane flames. In fact many works focus on the characterization of hydrogen enriched mixture for example the work of Noble et al. [12] and same results are reported by Figure 1-7. This figure shows the blowoff (squares) and flashback (dots) conditions; the ringed point shows a quick flashback cases. The flashback and blowout point are obtained obviously for different velocity but they are reported on the same graph to emphasize the different influence of hydrogen on this phenomena.

The increment of hydrogen concentration permits to reduce the equivalence ration before the blowout, this pattern is almost linear.

About the flash back the effect is limited for hydrogen concentration below 60% but over the influence is very high, in fact the flash back is very quick.

The stable range is divided into two regions: under 60% and over 60% of hydrogen. In the first one the operability could be enough for a gas turbine.

In the second region the range is reduced by the high H2 concentration and for the pure hydrogen is very narrow. For this reason the pure hydrogen fueling in lean premixing gas turbine isn't used in industrial application.

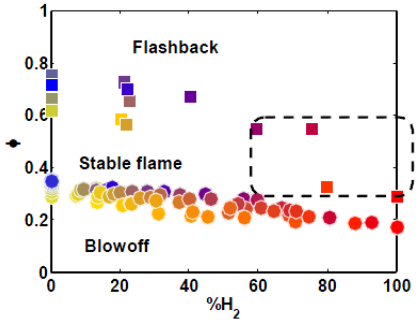

Figure 1-7: LBO (U0=6m/s) and flashback (U0=2m/) Vs H2 mole fraction and Equivalent ratio. Temperature: 460 K and pressure 0,44 MPa.

1.4 Auto ignition

When the characteristic premixing time is lower than the ignition delay time the autoignition is avoided. The complexity of the aerodynamics in a gas turbine combustor is the problem for a correct evaluating of the premixing time. Generally the temporal scale of the mixing in a lean premixed combustor is about 1-5ms.

Lieuwen et al. [13] reports a little difference about the ignition delay time between the methane and the hydrogen for the typical gas turbine temperature (from 600 to 1000 K).

The same result is reported by Therkelsen et al.[14], see Figure 1-8, they use this information to design their combustor in a micro gas turbine.

The main issue is the higher influence of temperature on the delay time in the hydrogen case than the methane one.

The pure hydrogen is theoretically safe about the auto ignition for the gas turbine operative condition. The ignition delay time is from 10 to 100 ms, and this time could be enough for a well designed combustor. The problem is the evaluation of this time because this result derived from an analysis of kinetic chemistry with mono dimensional model and it isn't enough validated.

Many innovative technological solution for the hydrogen fueling work with very little residence time. Marek et al. [15] propose the Lean Direct Injection "LDI" technology based on multiple injection points and quick mixing. The experimental activity shows that the flame ignites very near to the injection point and only a ceramic material is able to stand the high temperature.

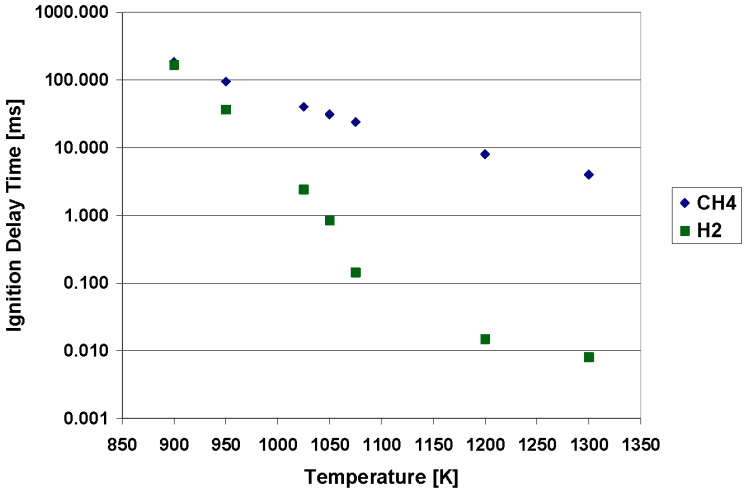

Figure 1-8: Ignition delay time H2 Vs CH4 [14]

Chapter 2.

Prototype design

2.1 Intro

The described work in this thesis is based on the investigation of a hydrogen fueled premixer prototype, thus this chapter writes about the unit development and the used tools. The first part describes the numerical model used for the development. The description starts from the diffusion flame modeling because the first hydrogen applications in gas turbine were on a non-premixed system thus this flame type is the reference point for the first part study. Next this approach was extended to consider the partial-premixed flame.

The second part of the chapter reports the development phase with the preliminary verification with numerical simulation before the experimental analysis, that will be described in the Chapter 3.

2.2 Computed Fluid Dynamics tool for combustion analysis

The intent of this thesis is the study of the hydrogen combustion in gas turbine regime. For this reason about the numerical tool the choice was the selection of a commercial code and not the development of a specific tool.

The selected code is Ansys Fluent, the oldest CFD code for the combustion analysis. The main characteristics of this code are the high number of available models for the flow, the combustion and pollutant evaluation. The description in this chapter is focused only to the combustion and pollutant modeling. During the course of full study all versions from 6.3 to the 14.0 were tested and used, but in this chapter the reference version is the 12.0.

Combustion Model

Modeling a typical gas turbine combustion process requires a turbulent combustion model to reproduce the interaction between chemistry and turbulence, it is formed by a turbulence model and a chemical model for the definition of the chemical species and their reactions.

Barlow and Carter [3] have shown that a non-premixed hydrogen turbulent flame with steady state boundary conditions is characterized by very complex structure and chemical kinetics. So, the choice of the combustion model must be made carefully. The commercial code used in this work for numerical simulations contains different combustion models, some specific for non-premixed flames (like the mixture

fraction-equilibrium model, the laminar flamelet model, and the Monte Carlo PDF model), and some specific for partially premixed flames and other models for generic reactions like EDC.

The Monte Carlo PDF model treats reaction exactly and evaluates PDF considering physics and chemistry of the system [16,17]. However, such model has two main disadvantages:

1) It's very computationally expensive (it's currently affordable only for reduced chemistry [18,19])

2) It requires the modelling of the molecular transport.

Also the EDC model is rather computationally expensive because it solves so many transport equations as the chemical species included in the kinetic mechanism. Besides that, the EDC model can produce mean temperature's spurious peaks in the reaction zone [16].

For all the above mentioned reasons, the Mixture Fraction-equilibrium and the Laminar Flamelet models seem to be the more appropriate, among the available combustion models, for the industrial combustor analysis. They allow the simulation of complex chemistry in complex geometries using pre-processing tables for the evaluation of temperature and chemical variables. The assumed PDF method used by the Laminar Flamelet model (the mixture fraction model is very similar) works reasonably well for non-premixed combustion [20]. In the mixture fraction approach, chemistry is modeled in a less accurate way than in the laminar flamelet one (only the equilibrium is considered) but this model results less computationally expensive and above all some CFD commercial codes don't require the user to implement the equilibrium kinetic mechanism.

The non-premixed modeling approach is based on a simplifying assumption, the instantaneous thermo-chemical state of the fluid is related to a conserved scalar quantity known as the mixture fraction, *f.*

$$f = \frac{Z_i - Z_{i,ox}}{Z_{i,fuel} - Z_{i,ox}} \qquad \textbf{2-1}$$

Zi mass fraction of element, i.

ox: the oxidizer stream inlet

fuel: the fuel stream inlet

The mixture fraction is a scalar linked to the local composition. Its values progress from 0 to 1; the value 0 is in the air stream and the value 1 for the fuel one. The sheet flame is where the mixture value is equivalent of the stochiometric one.

In the simplified model the F_{avre} mean (density-averaged) mixture fraction is considered and its transport equation is:

$$\frac{\partial}{\partial t}\left(\rho\vec{f}\right) + \nabla \cdot \left(\rho\vec{v}\vec{f}\right) = \nabla \cdot \left(\frac{\mu_t}{\rho_t}\nabla\vec{f}\right) \qquad \textbf{2-2}$$

About the interaction chemistry – turbulence the code applies the β-function shape probability density function (PDF) approach as its closure model. In order to take radiation into account, non adiabatic pre-processing tables were used.

The investigated technology isn't based on a pure diffusion flame but on a partial premixed flame. In premixed flames the sheet position is

also controlled by the equilibrium between the flow velocity and the flame velocity; for these reasons the combustion modeling includes Thin Flame Closure (TFC) model by Zimont [21,22].

The premixed combustion model assumes that the laminar flame is thinner than turbulent flame brush and it considers the reacting flow field to be divided into regions of burned and unburned species, separated by the flame sheet. The main variable is the C, where its value progresses from 0 to 1. 0 unburn, 1 full burned.

Its transport equation is:

$$\frac{\partial}{\partial t}(\rho\bar{c}) + \nabla\cdot(\rho\vec{v}\bar{c}) = \nabla\cdot\left(\frac{\mu_t}{Sc_t}\nabla\bar{c}\right) + \rho S_c \qquad \textbf{2-3}$$

Where the mean reaction rate is modeled as:

$$\rho S_c = \rho_u U_t |\nabla_c| \qquad \textbf{2-4}$$

P_u= density of unburn mixture

The expression of turbulent flame speed "U_t" evaluation [21] is

$$U_{t=} A u' \left(\frac{\tau_t}{\tau_c}\right)^{\frac{1}{4}} \qquad \textbf{2-5}$$

A: costant

u': RMS Velocity [m/s]

τ_t: turbulent time scale

τ_c: combustion time scale

At this point there are two model a pure premix and a pure diffusion model, the last needed element is a equation to join them to evaluate the local scalars:

$$\bar{\phi} = \bar{c}\int_0^1 \phi_b(f)p(f)df + (1-\bar{c})\int_0^1 \phi_u(f)p(f)df \qquad \textbf{2-6}$$

ϕ= is a local scalar as temperature, species fraction…

b:burned

u:unburned

Equation 2-6 is the closure equation that links the pre-calculated values from the PDF tables with the local value of "C" premix and "*f*" mixture-fraction. About the kinetic mechanism in this part of the work the "Hydrogen37" proposed by Peters and Rogg [23] was selected, this mechanism contains 13 species and 37 reactions. This is a reduced skeletal mechanism and it isn't optimized for a specific application range thus we are able to use it for many different cases.

In many cases the selection and validation of a mechanism is performed by the evaluation of laminar flame speed as in Campelo et al. [24] or Ströhle et al. [25]. In Fluent the code uses a function of laminar flame speed for pure hydrogen fueling and it isn't evaluated by the kinetic. In this case the laminar flame speed is obtained from numerical simulations proposed by Gottgens et al. [26]. The purpose of the mechanism is the local evaluating of species and heat release.

NO emission evaluation

NOx chemistry is too slow to be accurately represented by the laminar flamelet model: the use of a specific modeling tool is required for the accurate evaluation of NOx. In the present case of hydrogen combustion, only the NOx production from the intermediate N2O and the Zeldovich mechanism will be considered. The tool used in this work, previously tested and validated by Marini et al. (2010a) and Marini et al (2010b)), is a postprocessor of the reactive simulations solving only one transport equation for NO. NOx chemistry and turbulence interaction was modeled using assumed shape Probability Density Function (PDF) distributions of temperature.

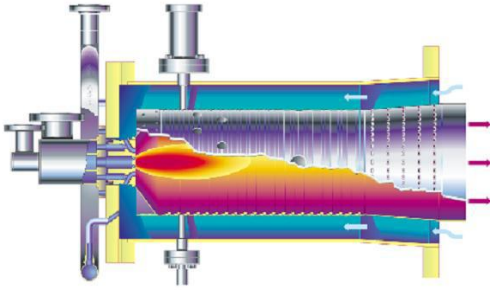

Figure 2-1:Combustion chamber under investigation

The validation of the model was performed on a diffusion flame combustor from a heavy duty gas turbine [27,28]. Figure 2-1 shows a schematic view of the combustor. The combustion chamber is a reverse-flow single-can design equipped with a diffusion flame burner. The working pressure, the inlet temperature and mass flow rate of fuel and air, and the air splits were imposed to the numerical simulations as

boundary conditions from the experiments. The experimental data available for the validation of the numerical analyses are NO_x and H_2 concentrations, which were measured at the transition piece exit section. The transition piece was not included in the solid domain in order to reduce the computational costs and to speed up the numerical simulations. It can be noted that in all cases, CFD underestimates NO (Table 2-1). The CFD and experimental data about NO_x emissions are not relative to the same combustor positions in the CFD calculations NO_x concentrations were evaluated at the liner outlet. In addition, the CFD simulations show that at the combustor outlet (where NO_x concentration is calculated) there are hot spots with temperature close to 2000 K. Therefore, it can be expected that a small but not negligible amount of NO_x is generated within the transition piece. Besides that, H_2 concentration on the combustion chamber exit section results to be zero in all the numerical simulations, as in the experiments.

Thus, the agreement between the CFD and experimental data can be considered satisfactory.

			NO_x ppm@15%O_2		
LOAD	**1/AFR**	**T air [K]**	**EXP**	**CFD**	**% (EXP-CFD)/EXP**
90%	0,0076	692	693	656	5
90%	0,0081	649	672	563	16
90%	0,0083	624	579	495	14

Table 2-1: Experimental vs numerical NO_x concentrations at the combustor discharge

2.3 Preliminary study

The premixer prototype under investigation derives from a DLN combustor, designed for natural gas, installed on a 120 MW FIAT heavy duty gas turbine. The original premixer was featured by an axial swirler and cross-flow fuel injection system, Figure 2-2. The swirler was composed by eight blades with a mean outlet angle of 24° degree with respect to the axial direction. This kind of swirler (swirl number 0.24) was not able to produce a stable toroidal recirculation zone at premixer's outlet.

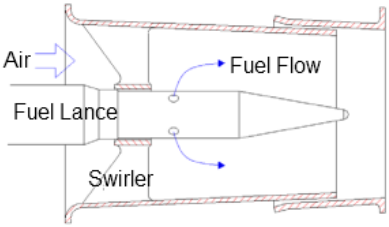

Figure 2-2: Original premixer

The fuel is injected through four holes made on a central lance and located on a plane close to the swirler outlet section; their distance from the burner exit was approximately equal to one premixer diameter. A first RANS CFD model was built to support the premixer redesign. The model prediction capability was validated in isothermal condition by comparing numerical data and experimental measurements performed by Hot-Wire probe (Figure 2-3), [29].

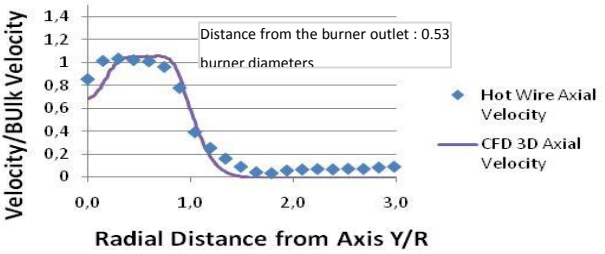

Figure 2-3: Axial velocity profile of the original premixer- comparison between hot wire measurement and CFD

The original unit was investigated in a short combustion test campaign in natural gas fueling, in this study the premixed showed a instable flame [29], see Figure 2-4.

Figure 2-4 : The instable flame, in the bottom the pilot torch used to stabilize the flame

2.4 Design

In order to obtain a stable flame, a new swirler characterized by a wider mean outlet angle (43°, Sn=0.7) was designed and built [30,31]. The new geometry was verified through CFD simulations in order to check the presence of the recirculation zone at the premixer outlet and to verify the flow/turbulence inside the premixer duct due to the new swirler geometry, Figure 2-5.

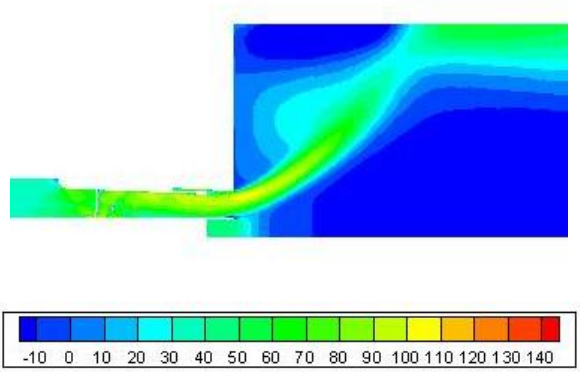

Figure 2-5: Axial velocity map [m/s] on a longitudinal plane. New swirler preliminary version

A new co-flow injection system [14] was designed to prevent the formation of high turbulence regions typical of the cross-flow interaction. The new injection system was composed by eight lances which pierce the swirler blades, Figure 2-6. The fuel lances were movable along the axial direction, to change the fuel delivery point and consequently the mixing level.

Figure 2-6 : A picture of the burner prototype

The CFD simulation of the first version, showed that in case of 100% hydrogen supply, fuel ignite in the premixer duct, see Figure 2-7. To overcome this problem a demountable ogive fixed on the burner exit was designed and built to increase the premixer outlet velocity and limit the flash back.

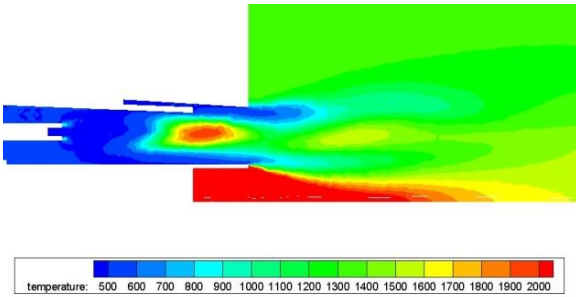

Figure 2-7: Temperature [K] field on periodic plane. New burner preliminary version

The new injection system with the ogive was investigated by means of detailed CFD simulations focused on the air/fuel mixing process. Figure

2-8 shows as the new premixer duct was able to guarantee a proper air/fuel mixing at its exit section.

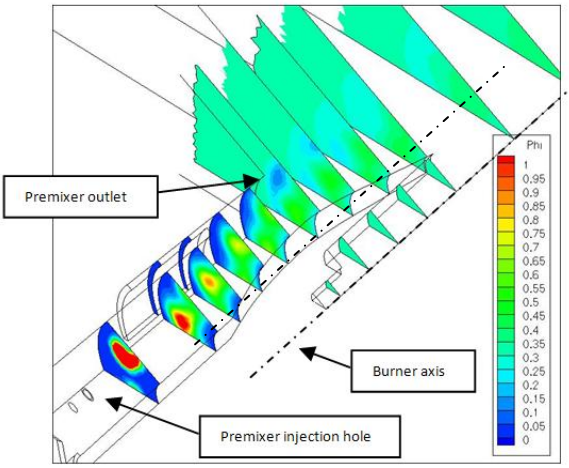

Figure 2-8: Equivalence ratio [-] maps on several crossing-sections of the burner prototype

To extend the operating range of the premixer, a commercial pilot burner was installed on the premixer axis instead of the original premixer injection lance. The schematic drawing in Figure 2-9 shows the main components of the developed burner prototype.

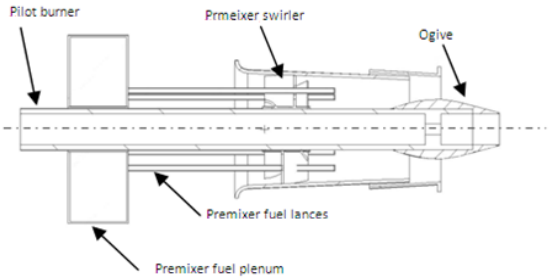

Figure 2-9: Schematic drawing of the burner prototype

The nominal/reference operative condition of the burner prototype (Table 2-2) was defined maintaining an unchanged premixer equivalent ratio, air temperature, burner discharge velocity of the original TG50 DLN premixing system operated at full-load with natural gas.

Premixer air flow rate	*g/s*	109
Premixer air temperature	*°C*	380
Premixer fuel	-	NG
Premixer fuel flow rate	*g/s*	2,8
Premixer thermal load	*kW*	132
P/T	*%*	6
Pilot air flow rate	*g/s*	2,5
Pilot fuel	-	NG
Premixer discharge velocity without ogive	*m/s*	67
Premixer equivalence ratio	-	0,44

Table 2-2: Nominal operating parameters of the burner prototype, NG fueling

2.5 Pre-test CFD analysis

Before starting the test campaign, the burner prototype in the final version was verified again by CFD simulation. The operating conditions of this simulation are given in Table 2-3. Aerodynamic flow field both for the premixer duct and the combustion region as well, shows a proper pattern as expected from the design activity.

Working pressure	atm	1
Premixer air flow rate	g/s	175
Premixer air temperature	°C	380
Premixer fuel		H2
Fuel flow rate	g/s	1.72
Premixer thermal load	kW	206
P/T nominal	%	0
Pilot air flow rate	g/s	2,5
Premixer discharge velocity (with ogive)	m/s	130
Premixer equivalence ratio "Φ"	-	0,35

Table 2-3: Reference Operation parameters for the burner prototype 100% H2 fired

Figure 2-10 reports the axial velocity map plotted on a longitudinal plane containing the burner axis. Inside the premixer duct the flow is well aligned and free of recirculation. At the premixer outlet the new swirler is able to promote the formation of a typical recirculation zone (CTRZ) [31]. Iso-lines were outlined in the region featured by negative values of the axial velocity at the premixer outlet.

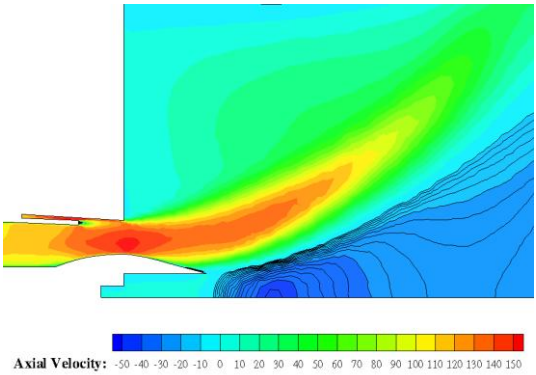

Figure 2-10: Axial velocity [m/s] map on a longitudinal plane with negative velocity iso-lines of CTRZ

Looking at the air-fuel interaction, Figure 2-11 gives some equivalent ratio maps, computed on crossing-sections at a rising distance from the fuel injection plane. The simulation showed a fairly homogeneous distribution of the equivalence ratio at the premixer outlet confirming the proper design of the injection system with regard to the air-H_2 mixing, too.

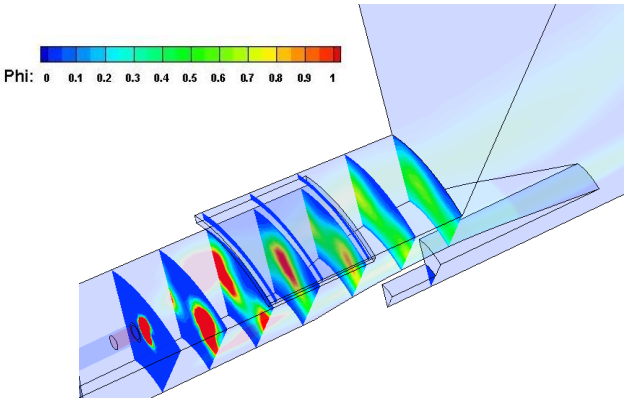

Figure 2-11 : Equivalence ratio [-] maps calculated on several cross-sections inside the premixer duct

Figure 2-12 shows the temperature map calculated on a longitudinal plane; cells with temperature values higher than 1600K are highlighted. Only a very small region has temperature values higher than that value, with a maximum value estimated around 1630K. It is the author's opinion that the CFD model slightly underestimated the flame temperature. Possible reasons could be the overestimation of both the air-fuel mixing and the distance of the flame front from the burner outlet section.

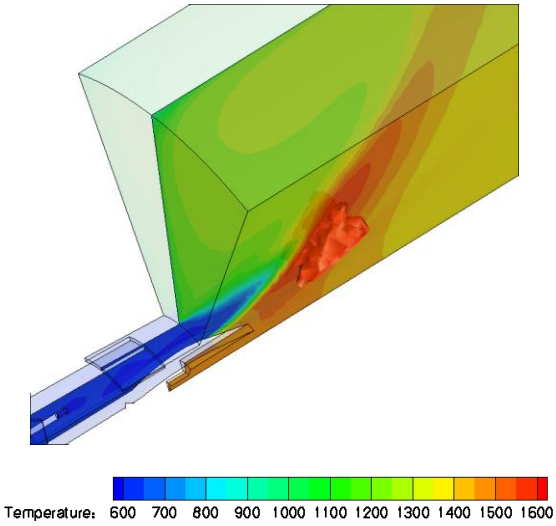

Figure 2-12 : Temperature map [K] on a longitudinal plane and cell region with temperature higher than 1600 K

Chapter 3.

Experimental characterization

3.1 Intro

This chapter describes the experimental campaign performed on the prototype. The intente of this study is characterization of the unit and data producing for the numerical approach validation.

This campaign was performed in collaboration with “ENEL Ingegneria e Innovazione S.p.A” division of electric company ENEL S.p.A..

After the description of test facilities and procedures the text reports the results about the temperature, OH chemiluminescence, NOx emission and operability. At the chapter’s end there is a comparison of experimental data with the result of numerical simulation performed in the design phase.

3.2 Test Facilities

The combustion test rig - named TAO (Turbogas Accesso Ottico – Turbogas Optical Entry) (Figure 3-1) - is installed in the ENEL's experimental area located in Livorno (Tuscany, Italy). This facility was built in 2004 with the aim to perform experimental investigations on gas turbine burners by means of advanced optical diagnostic techniques. Among several experimental campaigns performed up to now on the TAO facility, one of the most remarkable is the numerical-experimental study about thermo-acoustic combustion instabilities in lean premixed burner carried-out in the frame of PRECCINSTA European Program [32].

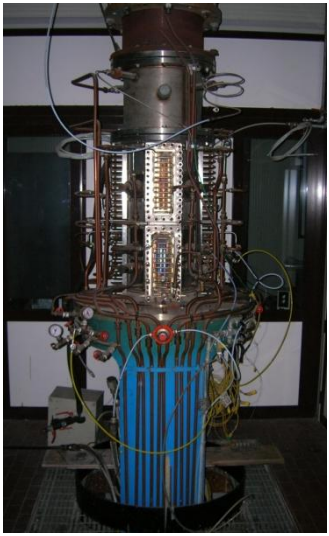

Figure 3-1 : The Combustion Test Rig

The rig consists of a vertical combustion chamber suitable for atmospheric pressure test of burners with a maximum thermal power input of 800 kW. Figure 3-2 shows a sectional view of the tested burner installed on the rig. Flat quartz windows used for optical access are installed on four walls of the octagonal chamber. The chamber, made in stainless steel, is 85 cm long with a 31 cm equivalent inner diameter ($2 \cdot r_c$, see Figure 3-2). At its end a conical shaped restriction leads to a downstream smaller chamber used for gas sampling and separates the combustion chamber from the exhaust discharge piping.

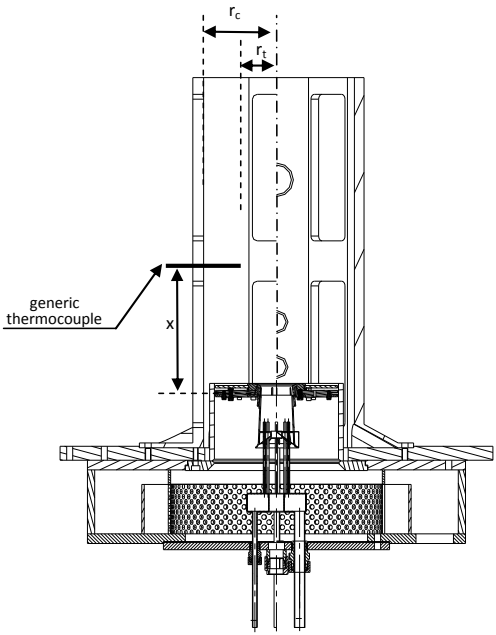

Figure 3-2: Combustion chamber section view

The combustion chamber cooling is done by means of ambient temperature air for the quartz windows and water for the metal walls.

The rig fuel system allows for supplying both gaseous and liquid fuels through three different lines. With regard to the test described here, premixed and pilot gas lines were used to supply the main and the pilot burner respectively.

Apart from the case of the natural gas operation, pressurized bottles were used for supplying pure hydrogen and hydrogen/methane mixture fuels. Air is supplied to the combustion chamber by means of two different lines. The first one is connected to the main fan and carries heated air to the plenum upstream of the main burner. The other supplies the pilot burner with air at ambient temperature.

For technical characteristics of the pilot it was fueled only with natural gas even in case with hydrogen fueling.

The combustion test rig is equipped with resident instrumentation, dedicated to air and fuel systems' control and necessary to ensure proper test rig operation. For test execution, the most important instruments are those providing mass flow measurements. Fuel mass flows have been measured by means of both standard orifices and flow meters. Pressure and temperature transmitters provide continuous monitoring of air and fuel supply conditions. The test hardware has been equipped with dedicated instrumentation in order to provide a detailed and comprehensive screening of the combustion system performances. Flue gas temperature inside the combustion chamber was measured by means of twelve thermocouples Pt-Rd type, installed along the chamber at a radial distance of 51 mm from the burner axis (see "r_t" in Figure 3-2 for details). Two 180 degree-shifted thermocouples were installed at the burner exit in order to monitor its metal temperature and to identify the flame flash-back onset. Two

sampling probe and a thermocouple were installed at the combustion chamber exit for measuring main species and flue gas temperature. NOx emissions were measured by means of both chemiluminescence and infrared analyzers, this unit gave ± 1 ppm in accuracy. Each test day it was calibrated with a certificated gas mixture.

Non-dispersive infrared analyzers are available for CO emission measurement, while oxygen content is measured by means of paramagnetic O_2 analyzers. The flame pattern has been obtained using the OH* chemiluminescence imaging. The OH* emission imaging highlights specific zones where heat release rates are supposed to be highest and carries out morphological and dynamic information of the flame.

The data acquisition of the test rig is performed by an electronic system that reads and stores the data from each sensor with 1 Hz frequency, the values are also visualized in real time. The mean values for each single test point were evaluated by averaging 30 consecutive acquisitions and checking the minimum, maximum and the STD values of this value set.

3.3 Experimental campaign

The intent of this investigation is the characterization of the prototype, the main variables investigated during the campaign are listed below:

- conventional pollutant emissions (NOx);
- flame pattern (via OH and gas temperature);
- burner operability (flash-back speed limit detection);
- burner pressure drop.

The above mentioned variables were assessed against the variation of operation parameters reported below:

- fuel type: natural gas, methane/hydrogen mixture (25%/75% in volume), pure hydrogen;
- premixer equivalence ratio;
- air velocity at burner exit;
- burner thermal load;
- air/fuel premixing degree.

These parameters were varied with respect to those of the nominal burner operative setting reported in Table 3-1, for the H2 fueling.

Premixer air flow rate	*g/s*	109
Premixer air temperature	*°C*	380
Premixer thermal load	*kW*	132
P/T	*%*	6
Pilot air flow rate	*g/s*	2,5
Premixer discharge velocity with ogive	*m/s*	81
Premixer equivalence ratio	-	0,35

Table 3-1: Nominal operating parameters of the burner prototype, H2 fueling

The prototype was analyzed with many arrangements but only few configurations were able to operate in hydrogen fueling thus the reported results are only for this configurations.

In the hydrogen fueled configuration the ogive was always present because the nominal outlet velocity wasn't enough to prevent the flashback. About the premix level only two injection positions were considered: the "Nominal", greatest permitted, and the "Low premix", where the fuel delivery point is in the middle of premix duct.

Test rig set-up

Preliminary test of the proper rig operation was done by comparing the oxygen concentration at the rig outlet with the value calculated through a mass balance based on operative conditions acquired by the facility control system. The same operation data were used as input of an energy balance for estimating the theoretical adiabatic temperature at combustion chamber outlet. The thermal power subtracted to the chamber by the cooling systems was then estimated comparing the measured temperature at the rig outlet with the value calculated from the energy balance. Data regarding the thermal power transferred to the cooling flows were used as boundary condition for the CFD model. Table 3-2 gives, for the tested fuels, the comparisons between oxygen and temperature values measured at the rig outlet with the calculated ones.

Fuel type	**Oxygen [% vol. dry conc]**		**Temperature [°C]**	
	Calculated	Measured	Calculated	Measured
NG	12,8	12,7	1302	910
CH4/H2	13,4	13,5	1326	880
H2	14,8	15,1	1356	900

Table 3-2: Rig mass and energy balance verification

In case of CH_4/H_2 mixture and pure H_2 fuels, whose chemical composition was certified by the bottle supplier, measured oxygen concentrations at combustor outlet were slightly higher than the calculated ones. This can be explained taking into account some air leakages into the chamber due to the window cooling. In the case of natural gas operation, the facility is directly connected to the gas national distribution pipeline. Due to large variation of the natural gas composition during the day, oxygen value calculated through the mass balance is affected by some uncertainty which can definitely explains the fact that the calculated oxygen is higher than the measured one. The comparison between the computed discharge temperature values and the measured ones allowed to estimated that the thermal power subtracted from the combustion chamber by the cooling systems was approximately equal to the 45% of the fuel thermal input.

3.4 Gas temperature distribution

The effect of the hydrogen content, thermal input, flow condition and mixing level on the gas temperature distribution along the combustion chamber was estimated by means of in-flame thermocouple measurement. Twelve thermocouples were positioned at increasing distance from the burner exit, their sensor being located at a radial distance of 51 mm (equivalent to 0.75 D) from the burner axis, see Figure 3-2.

In some cases the temperature profile will be reported in two form: dimensional and non-dimensional. The non-dimensional form is defined by equation 3-1:

$$T_{x-non-dim} = \frac{T_x}{\phi} - \frac{T_0}{\phi} \qquad \textbf{3-1}$$

T_x: Temperature of X thermocouple

T_o: Inlet air temperature

Actually this isn't a real non – dimensional form, because the results are a Kelvin quantity but it is able to helps to underline same interesting patterns of flame shapes.

Correction temperature value

Generally the data collected by thermocouples needs to be corrected by using a correlation in order to take into account of their energy radiation losses. When a thermocouple is in a high temperature zone, as in a flame, the radiation losses are important so the measured value is lower than the actual flow value. The difference can be over 200K in the higher temperature zone.

The equation 3-2, proposed by Kaskan [33], evaluates the ΔT between the actual flow value and the measured one.

$$\Delta T_{rad} = \frac{1.25\varepsilon\sigma T_w^4 D^{0.75}}{\lambda}\left(\frac{\eta}{\sigma v}\right)^{0.25} \qquad \textbf{3-2}$$

η: viscosity of air
ρv: mass flow
λ: thermal conductivity of air
σ: Stefan-Boltzmann constant
ε: constant = 0.22
T_w: temperature measured by the thermocouples

Figure 3-3 reports the comparison between the measured values and the corrected ones, the difference for temperature over 1000K is about from 130 to 180 Kelvin. However it is a author opinion that this expression underestimates the actual values because the temperatures are too low for a flame, in next chapters this conclusion was developed better with the numerical simulations support.

For the values of viscosity and thermal conductivity were used the temperature depended values of the air from open database.

The main issue of this equation is the "ρv" mass flow evaluating because without a CDF simulation is impossible knowing the local value, for the investigated case.

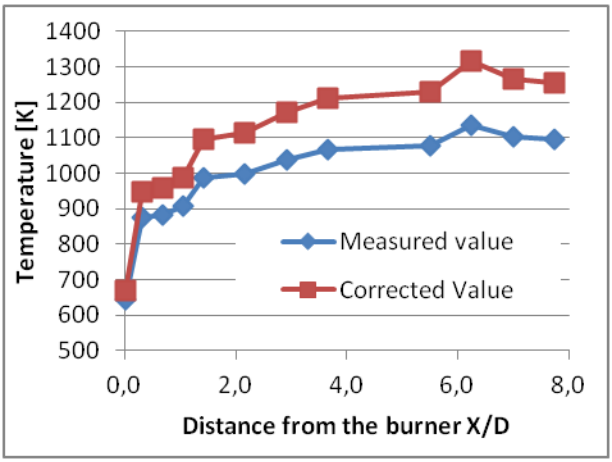

Figure 3-3: Temperature Profile: Measured Value Vs Corrected Value

An analysis of same reactive CFD simulations reports a constant value for "ρv" along the measuring profile for each case. In this work this correlation wasn't applied on full data set, because every case needs a CFD simulation, thus only in specifics case the correlation was used.

Influence of pilot presence

The unit is equipped by natural gas fueled pilot torch to permit the ignition but also to stabilize the flame. The second purpose was important for the natural gas fueling, in hydrogen fueling wasn't necessary thus the data set includes case with and without the torch using. When the pilot flame is put off, in the torch duct a small air flow

is present to protect the unit from high temperature. Figure 3-4 reports the temperature profile for two cases where the difference is the pilot flame presence. The image reports an unexpected result: the case with the pilot flame shows a lower temperature profile. The difference between the cases is small and it could be considered included in the systematic errors.

Figure 3-5 reports the effect of Pilot to Thermal ratio on the temperature profile, for the natural gas fueled configuration, and the result is similar of hydrogen case.

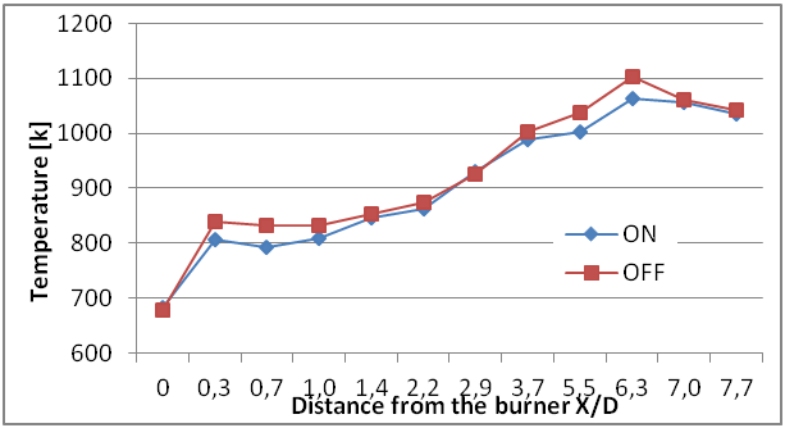

Figure 3-4: Pilot effect on the temperature profile, H2 fueling

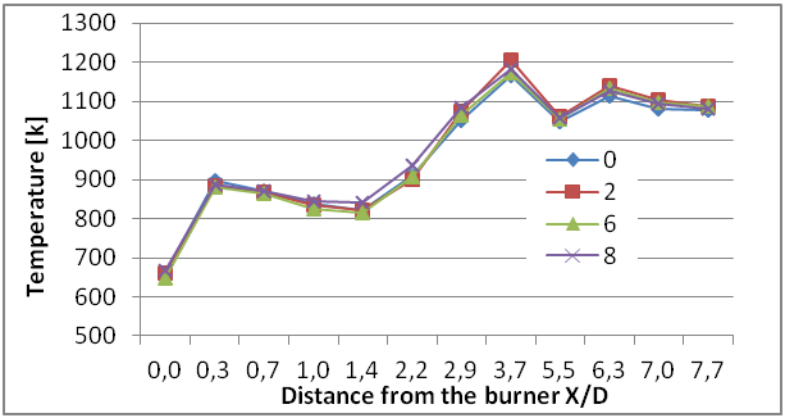

Figure 3-5: P/T effect on temperature profile, NG fueling

Equivalence ratio and Thermal input effects

The first explored set up was the case with the greatest premix level, for a safety operating the air flow rate had to be increased by 60% from the nominal value. From this safe condition the test explored the variation of gas flow rate with the fixed air flow rate.

This experimental set up permits to analyze the effect of thermal input and thus the equivalence ratio on the flame shape.

Figure 3-6 and Figure 3-7 report the temperature, in dimensional and non dimensional form, profile depending upon the equivalence ratio Phi. In this case the flame shape isn't influenced by the equivalence ratio and thermal input; Figure 3-7 shows the overlapping of the profiles. This result confirms the general roles of premixed combustion system that the flame shape is mainly controlled by the aerodynamic. This condition isn't reported for same case with natural gas fueling.

Figure 3-8 reports the non dimensional profile for the natural gas cases, with the nominal air flow rate 109g/s. In the middle zone the profiles aren't overlapped, in fact during the experimental activities the flame changed its shape, probably the main heat release was in the recirculation zone thus it influenced the aerodynamic.

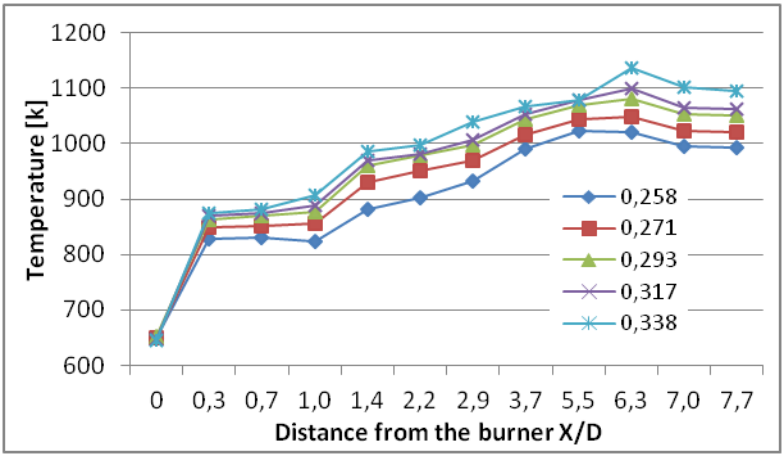

Figure 3-6 : Equivalence ration effect on temperature profile

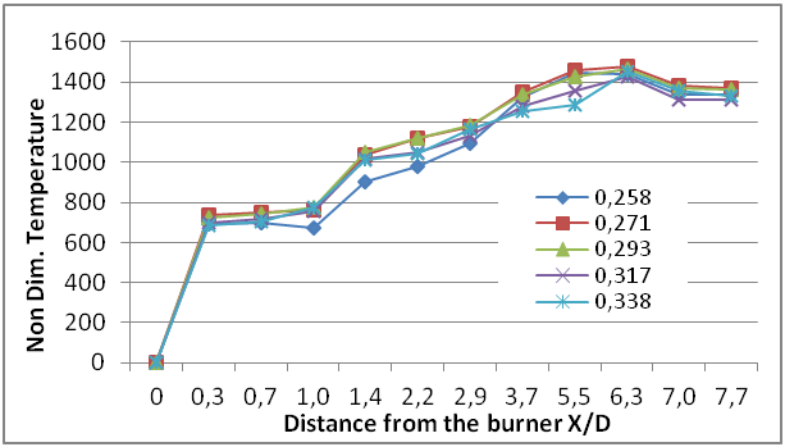

Figure 3-7: Equivalence ration effect on non dim. temperature profile

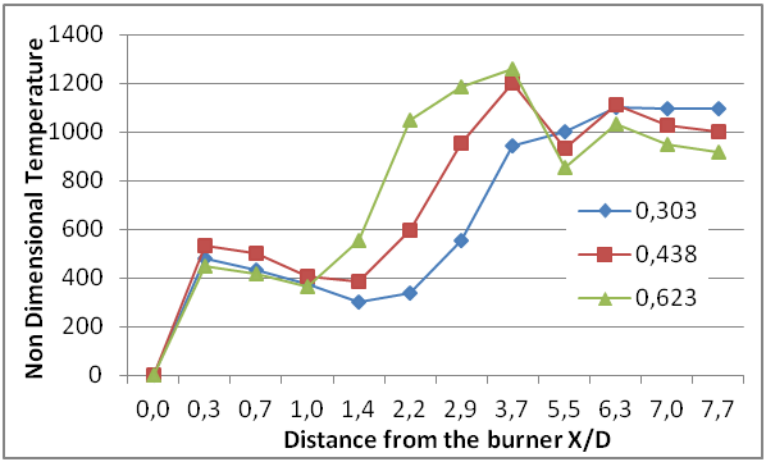

Figure 3-8: Equivalence ration effect on non dim. temperature profile, NG fueling cases

Air flow effect

The second explored case was a low premix configuration with the nominal thermal input, see Table 3-1. The premix outlet velocity is the variable quantity with a range from 84 to 122 m/s. The Figure 3-9 reports the measured values. On this data set the same non-dimensional analysis was performed as in the previous paragraph. In this case the data population was divided in two groups: the value over 100 m/s and the lower ones.

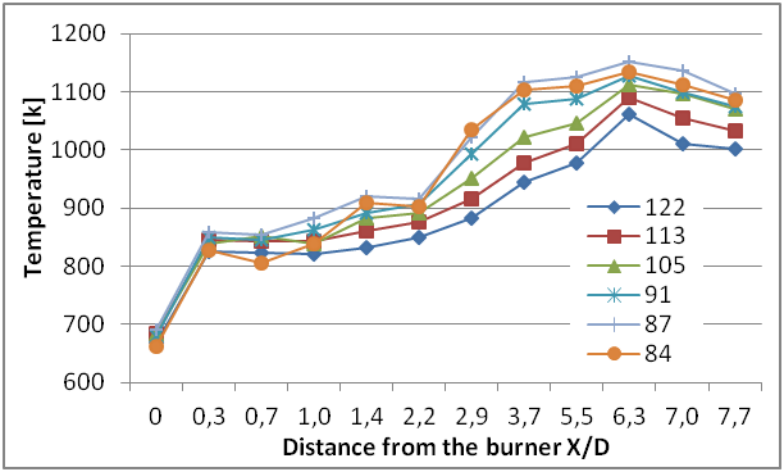

Figure 3-9: Outlet velocity[m/s] effect on temperature profile

The Figure 3-10 and the Figure 3-11 report the non dimensional analysis for each data groups. The cases with velocity over 100 m/s the flame presents a pattern opener than the lower 100 m/s cases.

The next elaboration reduces the analyzed X/D range, new one is from 0,3 to 6,3, and it calculates the average values for each data groups.

The Figure 3-12 and the Figure 3-13 show the results of this elaboration with its trend lines. The line of over 100 m/s cases is second order polynomial but the lower 100 m/s cases one is a third order polynomial.

The possibility to found a pattern in the flame temperature profile is a useful information for the comparison with the numerical simulation results, in this contest the validation procedure isn't only to hit a value but to reproduce a pattern.

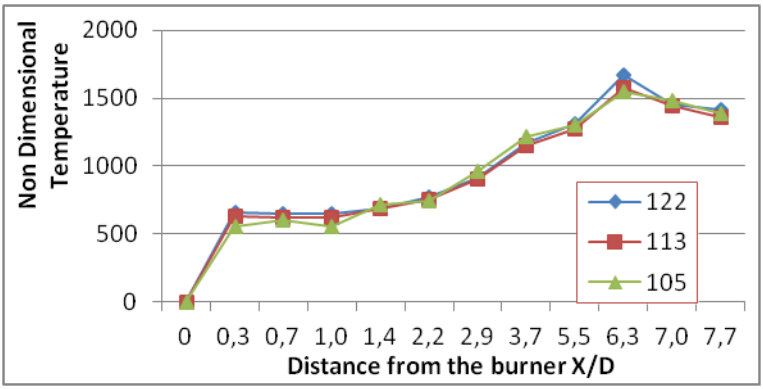

Figure 3-10: Outlet velocity [m/s] effect on non dim. temperature profile, over 100 m/s cases

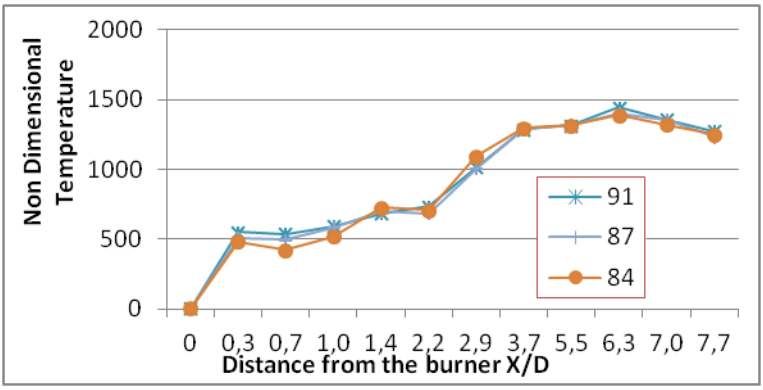

Figure 3-11: Outlet velocity [m/s] effect on non dim. temperature profile, lower 100 m/s cases

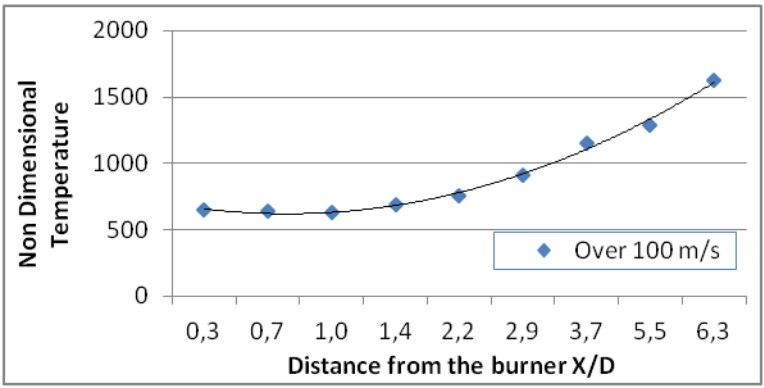

Figure 3-12: Average non dim. temperature profile, over 100 m/s cases

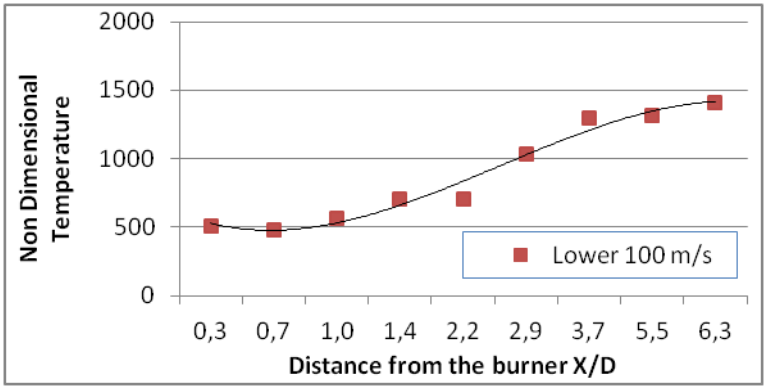

Figure 3-13: Average non dim. temperature profile, lower 100 m/s cases

3.5 OH Chemilunescence imaging*

Technique description

The OH* chemiluminescence imaging as diagnostic technique is relatively young, and it presents interesting capabilities [34,35] and for the hydrogen combustion, where the flame is invisible for the human eyes, it is a way to look the flame shape because the high concentration OH* individuates higher reaction rate zone [36,37].

The OH* evolution in a flame is governed by this simplified reaction scheme [38,39]

$$OH + O + M = OH^* + M \quad [R1]$$

$$OH^* = OH + h\nu \quad [R2]$$

$$OH^* + M = OH + M \quad [R3]$$

The reaction R2 is the cause of an emitting photon "hν" and it is the information acquired by the imaging system. This reaction could be also used for a laser stimulation.

Figure 3-14 shows the experimental set-up used for the OH* chemiluminescence imaging acquisition.

In this study only the natural emission was considered thus there aren't any stimulations.

The OH*–spontaneous emission, selected by the interferential filter at 310 ± 5 nm, was collected by a lens (UV Nikkor 105mm f/4.5) and focused on a imagine intensifier. The intensified imagine was carried to the CCD surface by a fiber bundle. The processed signal is sent to a PC

to acquire the flame image. The system allows for a variable acquisition frequency up to 100 frames/s.

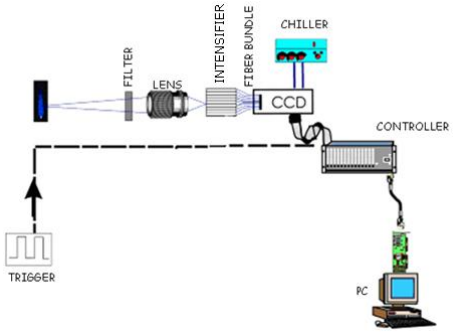

Figure 3-14: OH imaging experimental setup

Results

The OH* maps of the most meaningful configurations are given in Figure 3-15, each of them identified by a letter which defines the main operating parameters according to data reported in Table 3-3.

The heat release distribution of the first part of the flame was investigated by means of OH* chemiluminescence imaging technique.

The analysis of images reported in Figure 14 suggests the following remarks:

- the maximum reaction rate zone is located, for all configurations, on the interface between the premixer jet and the central recirculation zone;
- the pilot flame jet, visible on the burner axis zone, completely penetrates the internal recirculation zone;
- the heat release occurs mostly before the end of the observed window, i.e at a distance equal to two burner diameters;
- the increase of the air flow (keeping the equivalent ratio constant) does not change significantly the heat release distribution;
- in the three cases of hydrogen containing fuels, considerable flame moving back and shortening can be observed with respect to NG operation;
- the higher the hydrogen content in the fuel, the higher the maximum value of OH signal and the opening angle of the flame;
- in the case of pure hydrogen supply, the lowering of the premixing degree leads to a more extended OH emission zone.
- The flames aren't generally axial symmetric, probably high unsteady phenomena

Config.	Fuel	Burner	Air flow	Fuel flow	Premixing Level
A	NG	STD	NOMIN.	NOMIN.	NOMIN.
B	NG	OGIVE	NOMIN.	NOMIN.	NOMIN.
C	NG	OGIVE	+60%	+60%	NOMIN.
D	MIX	OGIVE	NOMIN.	NOMIN.	NOMIN.
E	H2	OGIVE	+60%	+60%	NOMIN.
F	H2	OGIVE	NOMIN.	NOMIN.	LOW

Table 3-3: Configurations investigated through UV imaging

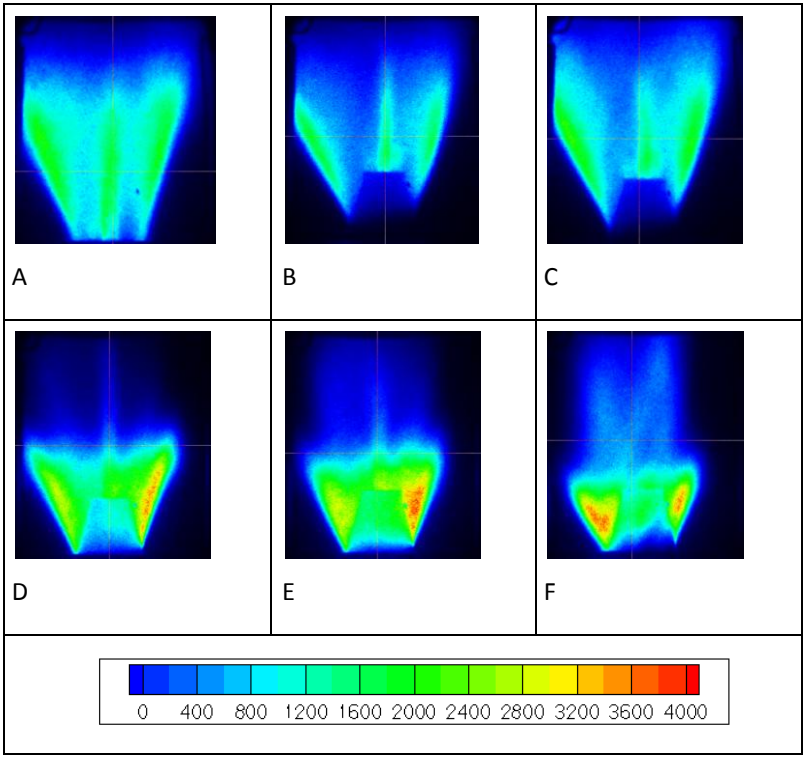

Figure 3-15 : OH distribution measured for configurations reported in Table 3-3

3.6 Pollutants

In hydrogen fueling the only emissions are nitrous oxides and the current experience in operative gas turbine [28,40] reports high values, incompatibles with current regulations.

During the experimental activities the NOx emission were measured for each explored configuration as the other quantities.

The Figure 3-16 shows the NOx emissions measured for the nominal configuration maintaining constant the air flow rate at the maximum value, see the paragraph 3.4, and changing the equivalence ratio by varying the fuel input, thus the thermal input.

For this set of data NOx emission are quite low from 6 up to 17 ppm @15%O2. In fact this configuration is characterized by nominal premixing and pilot flame switched off. On the other side the effect of the equivalence ratio is quite strong, about +11 ppm NOx for equivalence ratio from 0.258 to 0.338 (+13.7 ppm each +0.1 of ϕ) and the thermal input from 155 to 207 kW.

The graph of Figure 3-17 reports the results for the low-premixing configuration, with pilot switched on and varying the equivalence ratio by changing the air flow rate. The graph reports also the outlet velocity to emphasize the flow rate effect. In this case measured NOx emission were much higher due to the pilot contribution and to the poorest air/fuel mixing. The relation between NOx and equivalence ratio is, also in this case, about linear with a rate of +24.7 ppm each +0.1 of ϕ. Briefly considering all the configurations tested, NOx emissions are

quite low, from 5 up to 38 ppm@15%O2), also keeping in mind that combustion chamber rig is non-adiabatic.

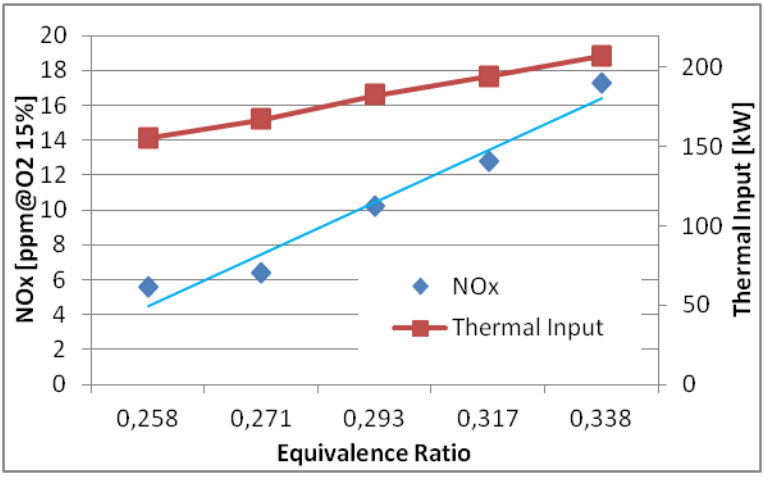

Figure 3-16: NOx emission Vs Thermal Input

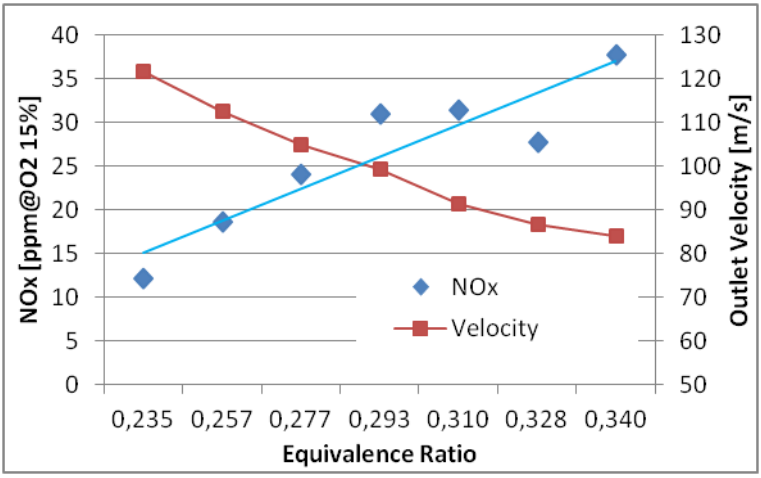

Figure 3-17: NOx emission Vs Outlet velocity

Concerning the effect of the air-fuel mixing level on pollutant emissions the parameters fuel-air mixture residence time and the segregation factor (S.F.), computed by the CFD simulations post-processing, were used. The residence time (τ) was estimated by the ratio between a reference mixing volume (V) and the mixture volumetric flow rate (Q); the reference volume is defined as the cylinder enclosed between the fuel nozzles and the burner exit.

$$\tau = \frac{V}{\dot{Q}} \qquad \textbf{3-3}$$

$$S.F. = \frac{std(\phi)}{\bar{\phi}} \qquad \textbf{3-4}$$

In order to estimate the effect of air-fuel premixing on pollutant emissions, gas lance position was shifted toward the burner exit, i.e, realizing different residence time and Segregation factor (S.F.) values. Figure 3-18 gives two test points with the same settings (air and fuel flow rate, ϕ=0.22, Tair=380°C, P/T=6) operated with two different fuel lances positions: the nominal and a different one with fuel supply near the outlet section, named low-premix. In this case, NOx emission are very low considering pure hydrogen combustion. The effect of premixing degree appears very important: the nominal point has about 3 times lower NOx emission with respect the low-premix arrangement. The nominal configuration has a residence time about 60% greater than the low-premix, this cause a better air/fuel mixing as outlined by the S.F. computed by CFD simulation, Figure 3-19. The S.F. for the nominal configuration is 82% of that for the low-premix arrangement.

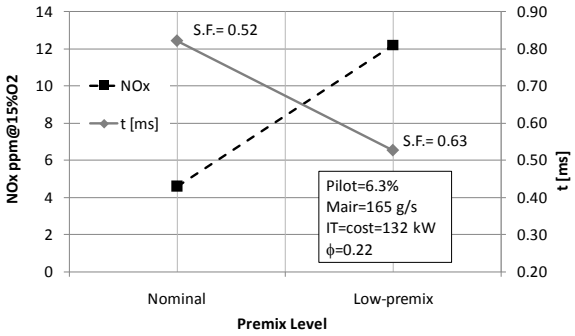

Figure 3-18: Effect of Premix Level on NOx emission (ϕ=0.22, pilot = ON)

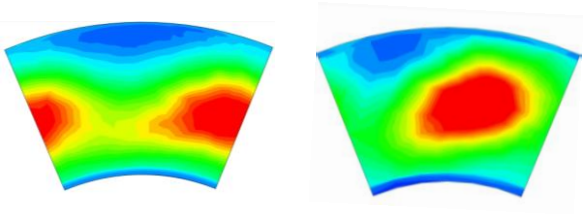

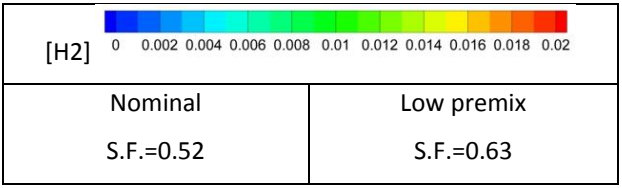

Nominal	Low premix
S.F.=0.52	S.F.=0.63

Figure 3-19: H2 mass concentration maps at the burner outlet, by CFD for Nominal and Low premix arrangements

3.7 Operability

The flash-back limit was investigated by changing step-by-step both the air and the fuel flow rate (keeping the equivalent ratio unchanged ϕ=0.22) until the flash-back was detected. Flashback onset was detected via UV camera signal which slightly anticipated the facility shut-down driven by the burner overheating protection, the latter being activated when the difference between the burner metal temperature and the combustion air temperature was larger than 15°C. The above mentioned investigations were performed for both arrangements nominal and low premix and the results are shown in Table 3-4. To guarantee a stable burner operation, the discharge velocity had to be increased up to 127 m/s for the nominal configuration. In case of low premix the limit discharge velocity decrease down to 87 m/s, but in this case the pilot was switched on. The higher burner exit velocity required to prevent flashback phenomena, leaded to a significant increase of the burner pressure drop, see Table 3-4.

Configuration	**Flash-back speed limit [m/s]**	**Pressure drop [%]**
Nominal	127	6.0
Low premix	87	3.3

Table 3-4: Flash-back speed limit and burner pressure drop

3.8 CFD Vs Exp

After the experimental characterization of the premixer a comparison with the CFD simulation, used in the design activity, is reported below. The CFD model predicted a typical "V" shape flame pattern for the simulated case. Quantitative information about the flame position can be outlined by means of the Progress Variable and its production rate analysis, which are the specific variables of the Zimont model [21,41].

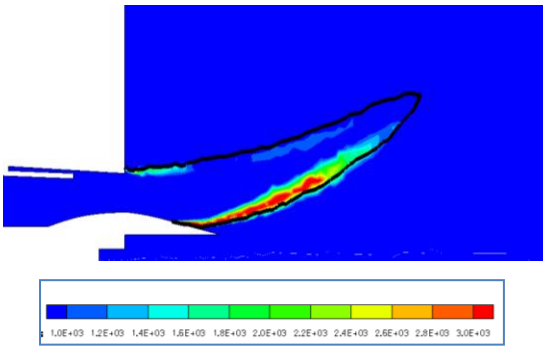

Figure 3-20 : Progress variable production rate on a longitudinal section with a 0,9 value iso-line of the Progress Variable

Figure 3-20 confirms the information about the heat release distribution coming from the experimental OH measurements, i.e the maximum reaction rate is located at the shear layer between the premixer outflow and the internal recirculation zone. With regard to the OH distribution estimation, it has to be noticed that measured (OH*) and numerical values cannot be directly compared. Despite this, a first preliminary analysis is here given comparing Figure 3-21 and Figure 3-22. In order to make the interpretation easier, the Figure 3-22

was reconstructed by coupling the OH* experimental map with the burner geometry, taken from the CFD geometric model.

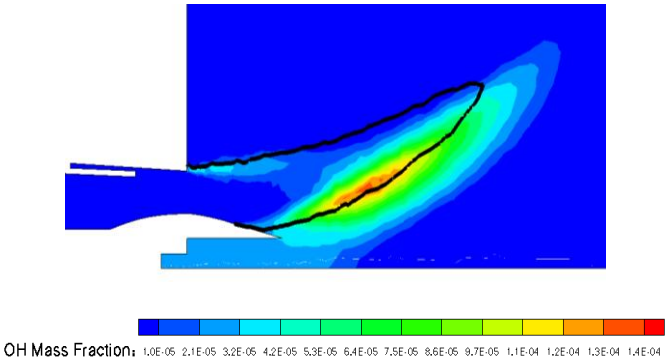

Figure 3-21 : Computed OH distribution with a 0,9 value iso-line of Progress Variable (Case "E" in Table 4)

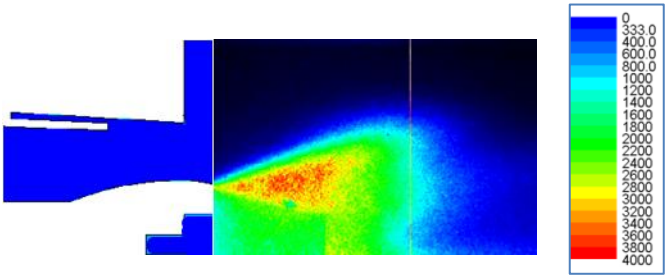

Figure 3-22 : Experimental OH* distribution (Case "E" in Table 3-3)

Both the model and the measurements highlight as the anchoring points of the flame are located over the ogive for the inner side and at the premixer external edge for the external one. Moreover, the CFD model predicts a flame shape wider in axial extension and shifted downstream with respect to that highlighted by the experimental results.

Chapter 4.

Numerical Unsteady analysis

4.1 Intro

The comparison of experimental data with the numerical simulation report a low agreement and the OH* chemiluminescence images show asymmetric flame. These results suggested the using of a unsteady approach for the numerical simulation.

Literature offers a large number of numerical approaches; of which Unsteady Reynolds Averaged Navier Stokes (URANS) and Direct Numerical Simulation (DNS) represent the opposite sides. When using DNS, all the turbulence scales are computed, conversely using RANS all the scales are modeled.

Large Eddy Simulation (LES) is an intermediate approach: large scales are computed while the smaller scales, up to the Kolmogorov ones, are considered as isotropic and then modeled by means of sub-grid models. LES represents the state of the art for the simulation of a number of components, but presents limitations connected to the amount of the necessary computational resources.

The most advanced application in turbo machinery analysis is represented by the work performed by Schlüter *et al.* [42], where a complete aero-engine was studied taking into account the interaction between compressor, combustor and turbine. Many industrial combustors have also been studied using LES, see [43,44] but the computational costs are high and the routine use of LES in industrial CFD is still impossible.

computational costs are high and the routine use of LES in industrial CFD is still impossible.

Hybrid methods are the most promising strategies for overcoming the limits connected to the diffusivity in the low Mach limit regime and to decrease computational costs. Amongst the hybrid LES/RANS approaches, Scale-Adaptive Simulation (SAS) is considered a second generation method [45] where the essential characteristics are the independence of the grid and the presence of a term which is sensible to the amount of temporal and spatial resolved fluctuations [46]. In this contest the SAS model is useful for the analysis of complex combustor geometry: in fact, SAS could reduce the computational time without neglecting important flow features [47,48].

4.2 Scale Adaptive Simulation Theory

Scale Adaptive Simulation - SAS is a high resolution method that has been developed by Menter and Egorov [49] and the basic idea lies on the development of the k-kL approach, originally presented by Rotta [50]. While Rotta models one of the source terms in the kL transport equation by means of a third-order velocity derivative, Menter and Egorov suggest modeling the same source term in a less restrictive but still physically acceptable way by using a second-order derivative. Therefore, the kL-form is transformed in a k-ω form where:

$$\omega = \kappa^{3/2} / kL \qquad 4\text{-}1$$

This term results in addition to the ω-transport equation of the SST model proposed originally by Menter [51]. The transport equations for the scalar quantities are listed in Eq. 2 and Eq. 3:

$$\frac{\partial \rho k}{\partial t} + \frac{\partial \rho U_j k}{\partial x_j} = P_k - c_\mu^{3/4} \rho \frac{k^2}{\Phi} + \frac{\partial}{\partial x_j}\left(\frac{\mu_T}{\sigma_k}\frac{\partial k}{\partial x_j}\right) \qquad 4\text{-}2$$

$$\frac{\partial \rho \cdot \Phi}{\partial t} + \frac{\partial \rho U_j \Phi}{\partial x_j} = \frac{\Phi}{k} P_k \left[\zeta_1 - \zeta_2 \left(\frac{L}{L_{vK}}\right)^2\right] - \zeta_3 \rho k + \frac{\partial}{\partial x_j}\left(\frac{\mu_T}{\sigma_\Phi}\frac{\partial \Phi}{\partial x_j}\right) \qquad 4\text{-}3$$

$$L_{vK} = \kappa \left| \frac{\partial U / \partial y}{\partial^2 U / \partial y^2} \right| \qquad 4\text{-}4$$

The definition of $\Phi = \sqrt{k} L$ (Eq. 4-3) and the values of the calibration parameters can be found in the original work by Menter and Egorov. In

the SAS approach, L is compared to the von Karman scale L_{vK} (see Eq. 4-4):the L/L_{vK} term allows the model to recognize the scales resolved in an unsteady flow and to correct the turbulent viscosity v_t. With respect to the Detached-Eddy Simulation (DES) approach, where RANS is used in the near wall region and LES elsewhere, SAS is able to define where to use LES depending on the mesh dimensions and on the flow characteristics. In conclusion, the most important characteristic of the SAS approach is that the local evaluation of the turbulent length scale allows smoothly changing the resolution from RANS to LES.

4.3 Setup

This activity focused on improving the individuation of the flame front in comparison to results obtained by the previously activities. Since the main gap between CFD and experimental data was considerable in the case of conditions near the flashback limit, the SAS model was tested in that condition. Figure 4-1 shows the premixer with details about the air and fuel inlet.

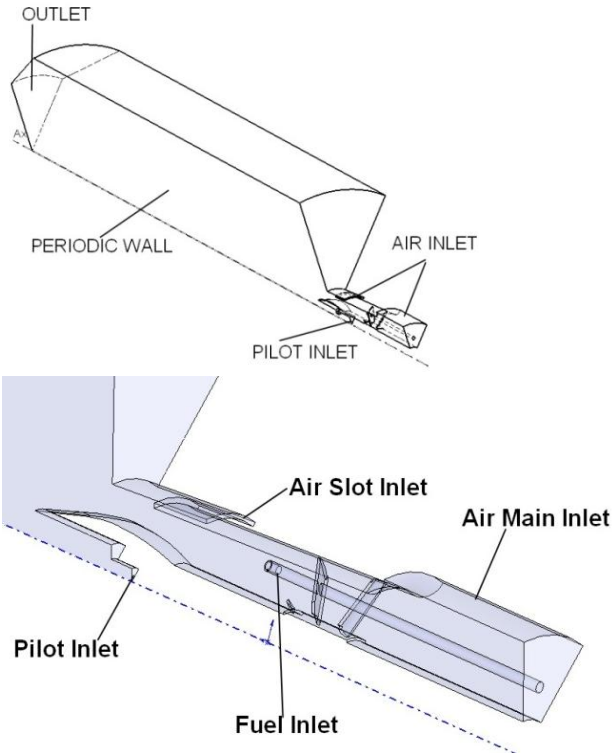

Figure 4-1 – Combustor model

The axial swirler, characterized by eight blades and eight fuel lances, defines the 45° rotational periodicity of the model as in the previous part of the this work.

Hybrid unstructured computational meshes were generated by means of the commercial code Centaur^{TM} (Figure 4-2). The grid is composed approximately by 6.9M elements with prismatic layers used for near-wall treatment and tetrahedral cells elsewhere. The maximum dimension of a tetrahedral element is 0.8 mm in premix and flame zone while it is 3 mm elsewhere. The mesh quality near the walls was controlled by the analysis of y^+ values.

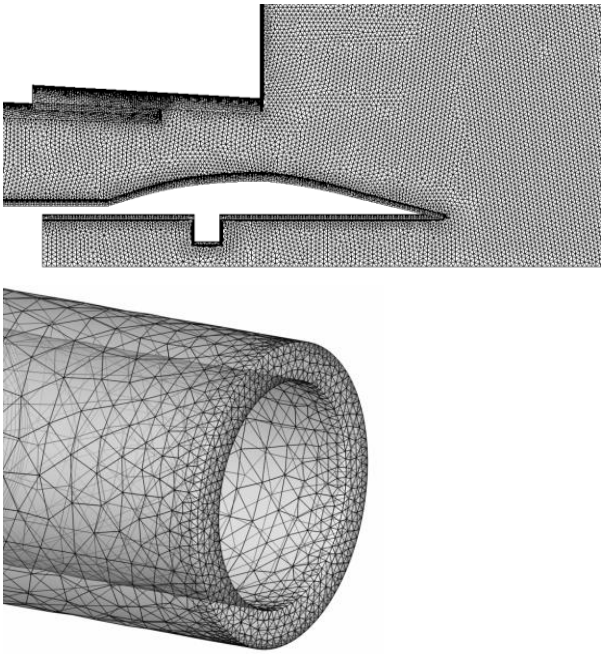

Figure 4-2 – Detail of computational mesh of the premixer and of the lance

Boundary conditions (Table 4-1) were imposed in terms of inlet mass flow rate and outlet static pressure. In the test rig, air inlets worked with the same total pressure, as a consequence this condition was reproduced in the simulations with an a posteriori check. The intensity turbulence level is quite low (around 1%), since a plenum is used in the test rig the turbulence level is consequently reduced.

Working pressure	atm	1
Premixer air flow rate	g/s	175
Premixer air temperature	°C	380
Premixer thermal load	kW	207
Premixer discharge velocity (with ogive)	m/s	127
Premixer nominal overall equivalence ratio "Φ"	-	0.338

Table 4-1: Boundary conditions

4.4 Results

The study was performed on 12 CPUs of the CINECA PLX cluster. With this hardware, 24 time steps were calculated every day and the calculation time was performed in many months. Therefore, the CFD analysis of the industrial combustor is not quicker than experimental analysis, although it could provide information on the actual behavior of the flow inside of the premixer, where the experimental results are few. In same case the comparison with the old RAN simulation are reported. The comparison with the RANS simulation performed with the same mesh is impossible because this simulation failed.

The failure was caused by the solution of turbulence structures, see Figure 4-3, that the RANS modeling isn't able to resolve. This phenomena is caused when the mesh is too detailed and the solver transform the simulation in a pseudo unsteady simulation.

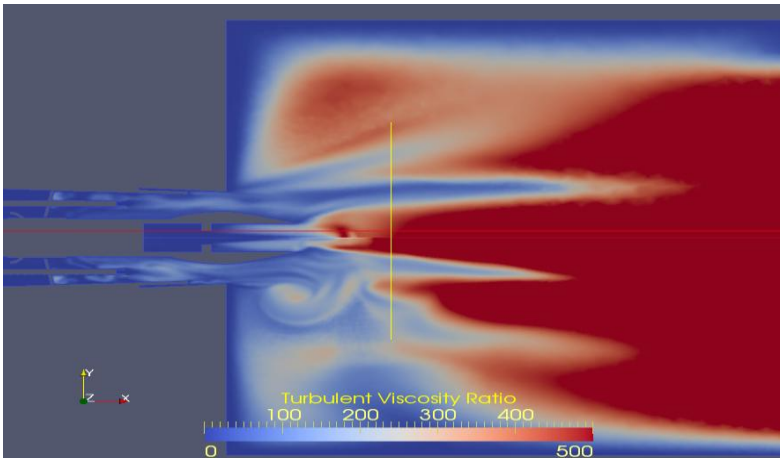

Figure 4-3: Turbulent viscosity ratio with different meshes, up the older and bottom the SAS mesh

Figure 4-4 shows the time resolved velocity magnitude maps obtained near the exit section of the premixer. It can be evidenced that inside of the premixer duct the flow is well aligned and free of recirculation. On the contrary, at the outlet section of the burner the typical recirculating flow structures are generated.

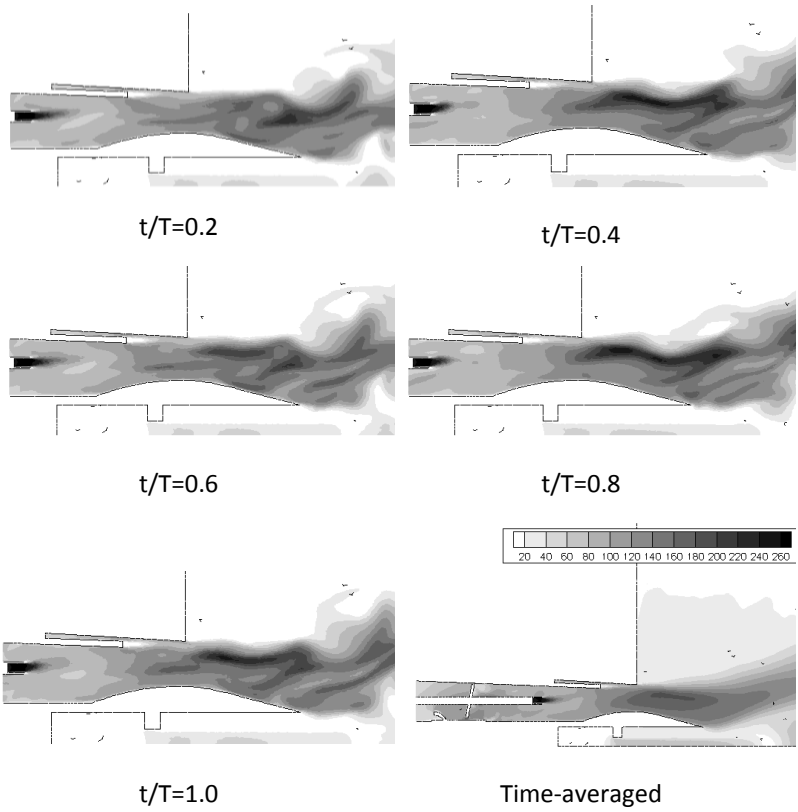

Figure 4-4 : Time-resolved and time averaged velocity magnitude on a longitudinal plane

The flow structures evidenced in Figure 4-4 were not visible from previously performed RANS calculations due to treatment of turbulence, as demonstrated by Figure 4-5 where the viscosity ratio field on the longitudinal plane is shown. RANS solution is almost uniform and presents higher (not physical) values than the SAS solution. In fact, SAS is able to resolve large eddies when the computational mesh is sufficiently accurate, as in this case. This characteristic of SAS is very important in combustion chambers, where turbulence plays a key role in the definition of the unsteady temperature field.

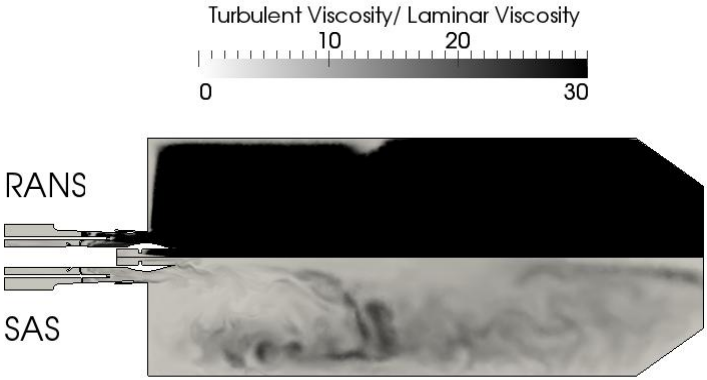

Figure 4-5 : RANS vs SAS: Viscosity Ratio

In the experimental activity the burner operated in secure state with the working conditions reported in Table 4-1. Also, RANS calculations did not evidence the presence of flashback, see chapter 3.8. Actually, the thermocouples that should alert in case of flashback are positioned in a region where the cold flow has a strong influence (Figure 4-6) and the detection of flashback could be delayed.

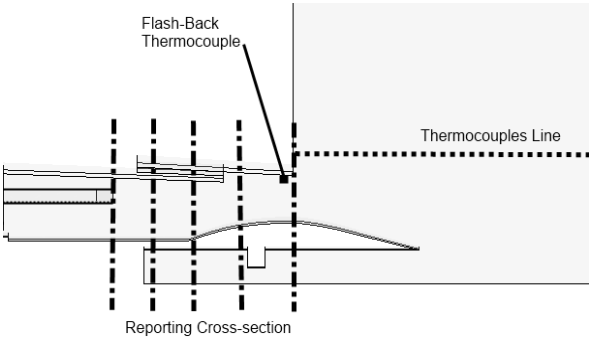

Figure 4-6 : Probes and cross-section positions

In fact, direct observation of the premixer during the experimental campaign allowed individuating flashback for the selected working condition, and then the use of SAS could provide more information on the actual flow field and on the RANS limited performance. Figure 4-7 and Figure 4-8 show the comparison of mixture fraction fields and progress variable on a longitudinal plane, respectively. The highest mixture fraction value (0.0321) represents the stoichiometric value. The mixing in the RANS solution seems to be over predicted and this could cause the late flame development evidenced by the progress variable in Figure 4-8.

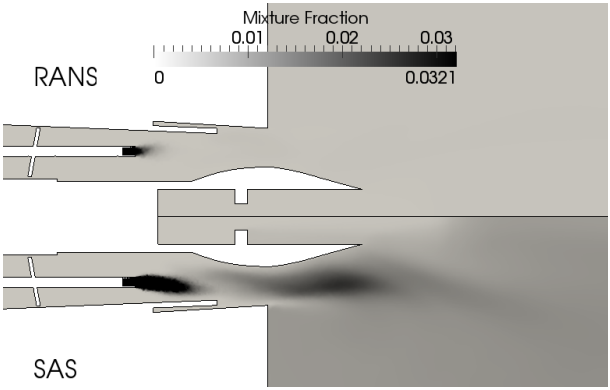

Figure 4-7: RANS *vs* SAS: mixture fraction on a longitudinal plane

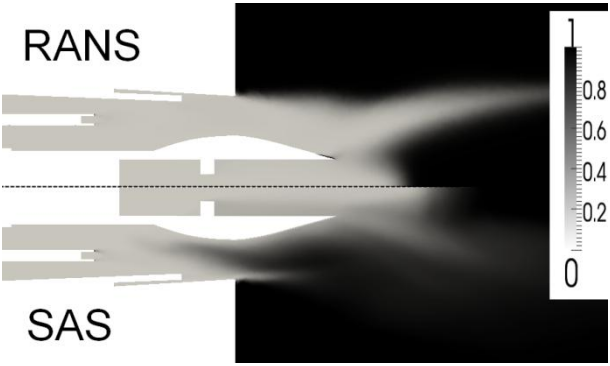

Figure 4-8: RANS *vs* SAS: progress variable on a longitudinal plane

Figure 4-9 shows the comparison of the experimental non-dimensional temperature profile with the SAS data, in this case the non-dimensional is referred to the outlet temperature.

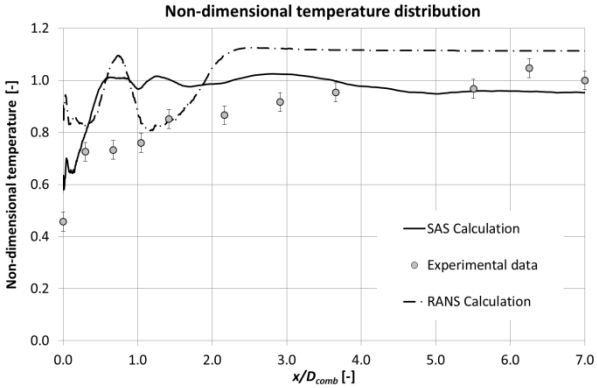

Figure 4-9: Comparison of non-dimensional temperature profile

Figure 4-10 reports six cross-sections of the mean premix variable in the duct obtained using SAS. The flame develops on a helical path; originally there are eight distinct flames one for each injection point, and only after the outlet do these flames join themselves. The fuel ignites near the injection point and the premix variable reaches a value of 0.8 in the duct determining a well-developed flame at the outlet. As expected, the temperature maps of Figure 4-11 show that the metal walls are protected from the flame by the air flow coming from the slot, it is why thermocouples were not able to individuate the flashback condition.

Figure 4-10: Mean progress variable, maps calculated using SAS on several cross-sections inside of the premixer duct

Figure 4-11: Mean temperature maps calculated using SAS on several cross-sections inside of the premixer duct

Concerning the production of pollutants, the numerical prediction of the thermal NO_x emissions showed a concentration of 1 ppm@15%O2, considerably lower than the measured one of 18 ppm@15%O2. It can be underlined that this result is coherent with the volume of high temperature zones (over 1900K), which is quite small. CFD results suggest that in this case the main mechanism of NO_x production could be different than Zeldovich mechanism.

Chapter 5.
Updated RANS modeling

5.1 Intro

After the unsteady analysis same aspects were uncertain about the flame shape and the path of NOx emission, the first because the experimental temperature profile was only partially reproduced, the second the post processor wasn't able to work properly.

However the unsteady analysis was too computational expensive thus a updated RANS modeling was proposed even if this method shows same limits.

The computational mesh was reconsidered, the initial validation was based on the velocity profile in cold flow, see chapter 2.2, because the experience on natural gas system reported this validation was enough. The unsteady analysis showed the limits of this way for the hydrogen fueled reactive flows.

The NOx evaluation is influenced by the temperature field thus it needs a correct evaluation of this field and it is possible only a good mixing evaluation.

The work focused on the individuation of other path for the NO production, in fact Bozzelli et al. [52] show the existence of the NNH way and Skottene et al [53] show its importance in hydrogen fuelling.

The chapter ends with a evaluation of pressure influence on flame shape and NOx emission. The experimental activities were performed only in atmospheric conditions but Leonard et al. [54] and Biagioli et al. [55] report the influence of the operative pressure on NOx emission.

5.2 Decoupled post processor for emission

In this study was used a new post processor for the pollutants evaluation because the previous tools was able to evaluate only the thermal path.

This tool is base on a stiff solver where a detailed kinetic was imported and elaborated; in this case the Gri-mech 3.0 [56] was selected. This tool is able to resolve many reactions, with low computational cost.

The post - processor uses the temperature field and all original species fields from the previous combustion simulation. For this reason the original simulation had to be resolved with a kinetics that didn't include the pollutant species.

For this reason the Li et al. [57] kinetic mechanism was selected for the previous combustion simulation, also it is optimized for the hydrogen combustion in atmospheric condition.

Each pollutant species are resolved by a specific transport equation. All un-pollutant species, in the detailed kinetic and not in the original simulation, are evaluated by a chemical equilibrium calculation at the fixed temperature of the original solution. The Gri-mech was developed for hydrocarbon fuels thus it includes species and reaction with carbon, the solver eliminates all these elements because they are unnecessary.

5.3 Solid model and computational mesh

Figure 5-1 shows a view of the premixer and the combustion chamber geometric model with details about the air and fuel inlet.

The original periodicity of 45° was modified to 90° to avoid the influence on the solution. In the Figure 5-1, two blades and two fuel injections are present in the solid model.

The experimental activities showed a very short flame thus the dimensions of the combustion chamber are reduced by 30% to reduce the computational cost.

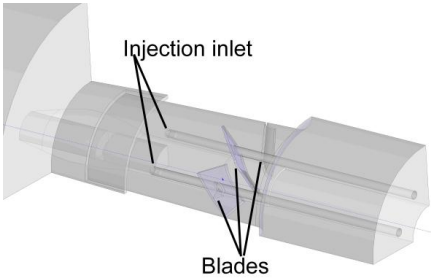

Figure 5-1: Detail of Solid Model, there is one complete blade and two half blades

The computational mesh, Figure 5-2, is hybrid non-structured and it was generated by the commercial code Centaur™ [58]. The grid is composed of 4.4 million of elements with prismatic layers used for near-wall treatment and tetrahedral cells elsewhere.

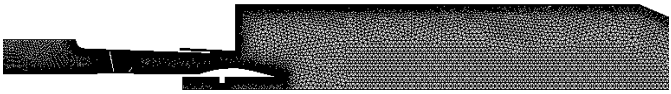

Figure 5-2 : Computational Mesh

5.4 Results

This paragraph reports the comparison with the experimental data and other interesting information that only the numerical procedure is able to show.

The selected analyzed point is the nominal point with low premixing setup and hydrogen fueled, see Table 5-1. This point is the only one of the low premixing series with the pilot switched off thus the flash back limit is little lower.

The same condition with the pilot switched on presented a full flash back., and it is the point reported in chapter 3.7.

The pilot is natural gas fueled and it is a problem for the numerical code because it isn't able to analyze two different fuels.

Working pressure	atm	1
Premixer air flow rate	g/s	113
Premixer air temperature	K	663
Premixer thermal load	kW	132
Premixer discharge velocity (with ogive)	m/s	84
Premixer nominal overall equivalence ratio "Φ"	-	0.340
Experimental NO emission	ppm@15% O2	38

Table 5-1: Boundary conditions

During the experimental activities the temperature profile in the flame was acquired; the measured values were corrected by using correlation proposed by Kaskan et al. [33] in order to take into account of the energy radiation losses, see chapter 3.4.

Figure 5-3 shows the comparison between experimental data and CFD, in dimensionless form, the dotted line in Figure 5-4 shows the position of thermocouples in comparison with the flame.

The numerical results present an acceptable agreement with the experimental ones, the trend is the same compared with the result of chapter 3.4 on the flame shape. In this case the flame shape is characterized by a third order polynomial.

The main difference is in the first points, near the metal wall, where the CFD results are higher than the experimental.

The test rig was cold but the cooling distribution wasn't well known, probably the heat exchange is more intense near the premixer where there is the air plenum. The uniform condition of the wall temperature used in the simulation is too limited.

Figure 5-4 shows the CFD temperature field on a longitudinal plane. The zone with a high temperature (>2000K) is little and compact, this condition influences the NO emission. The thermocouples position line is tangent with the high temperature zone for this reason the profile trend is monotonic and there aren't any peaks.

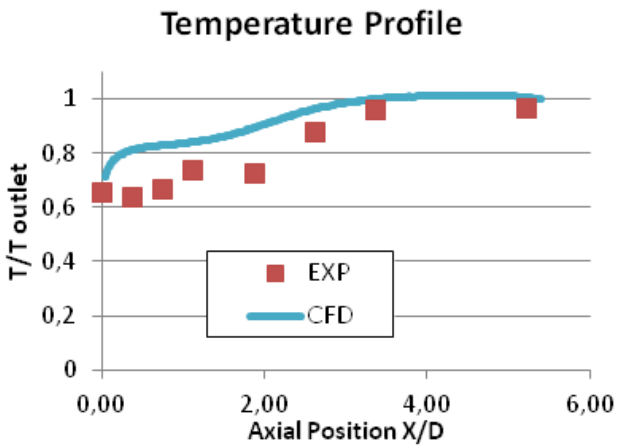

Figure 5-3 : Non-dimensional temperature profile. Exp Vs CFD

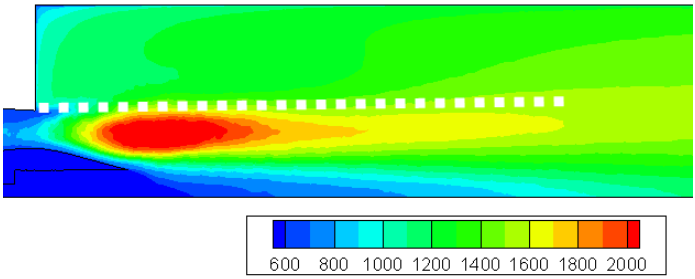

Figure 5-4 : CFD Temperature [K] field on longitudinal plane

Figure 5-5 shows the experimental OH* image and Figure 5-6 shows the Premix - C rate field on a longitudinal plane. The two images represent a similar information on the flame position, but using a different visualization method.

The flame position is well identified and the shape is similar in the same visible zone, see the white line, the experimental image shows

only a limited region of the flame, for example it isn't able show what happens in the premixer but the CFD is able to.

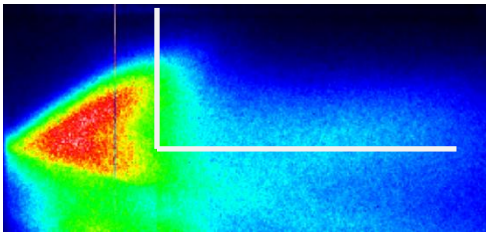

Figure 5-5 : OH Exp. Imagine

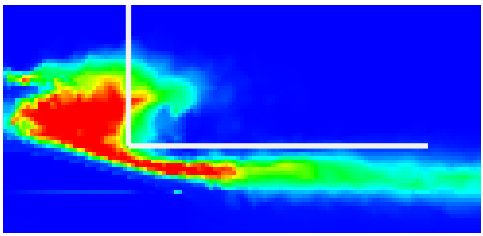

Figure 5-6 : Premix-C Rate from CFD

Actual flame shape

The Figure 5-7 shows the complete flame shape, in detail the flame is in the duct and the flame ignition is very close to the injection point.

The metal walls aren't involved by the flame, the cold air slot protects them.

The OH* chemiluminescence image wasn't able to show what happened in the duct. The flashback detection system in this operative condition didn't reports flash back, probably it was influenced by the cold air flow from the slot. This result is already reported by the unsteady analysis with a different accuracy, see chapter 4.4.

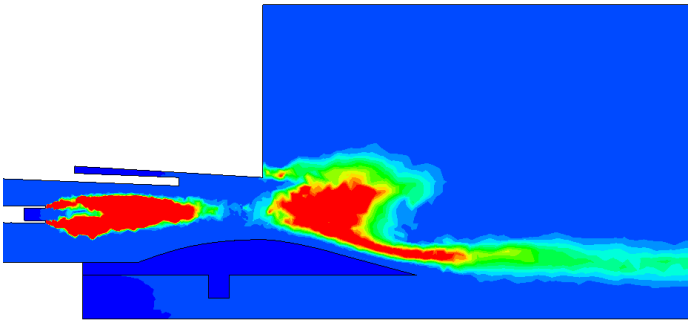

Figure 5-7 : The complete CFD image of Premix - C rate on a longitudinal plane

Figure 5-8 shows the actual 3D flame shape, four crossing planes in the duct are reported.

The early ignition doesn't permit the correct mixing, in fact the flame shape is very similar to a stretched diffusion flame ignited from each lance; the flame front is the boundary of gas with the air.

This unmixing condition exists with a 84 m/s discharge velocity and a high swirling component.

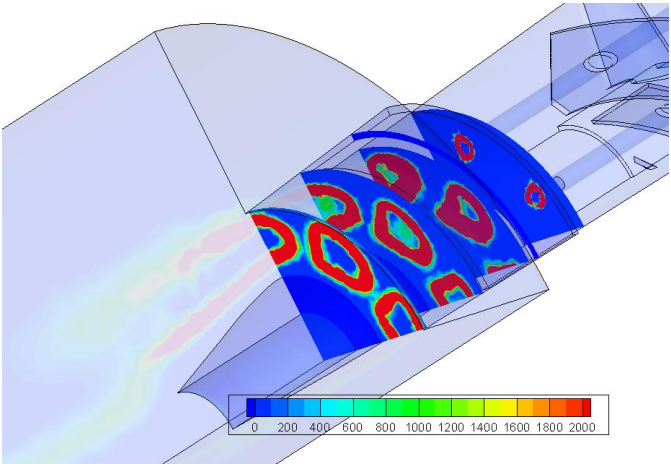

Figure 5-8 : Cross section of Premic-C Rate in the duct

NO emission

The NO is the only emission in the hydrogen combustion thus its evaluation is important. In this study three evaluation ways were considered: the pure Zeldovich postprocessor, as in chapter 2.2, the decoupled with a Zeldovich limited chemistry and the decoupled with a complete chemistry; Table 5-2 shows the results of this analysis.

	ppm NO @15% O2
Experimental	38.00
Pure Zeldovich - Post	9.59
Decoupled Thermal way	6.32
Decoupled All ways	41.00

Table 5-2 : Evaluation NO emission, Exp. Vs CFD

The value from the Decoupled post processor, with complete chemistry, is very close to the experimental value, 41 ppm NO @15% O2 vs 38 ppm NO @15% O2.

The other two cases, where the only thermal path was valuated, present a very low value in accordance with the temperature field. This result shows plainly that the thermal isn't the main way for the NO emission for this flame.

Skottene et al. [53] reports the importance of the NNH [52,59] way for the NO production in hydrogen flame.

The NNH way is significant when a high concentration of dissociated H2 and O2 are present in the flame, this condition is typically of the hydrogen combustion in air. The high level of H promotes the R1 reaction and the O promotes the R2 reaction.

$$N_2 + H = NNH \qquad [R1]$$

$$NNH + O = NO + NH \qquad [R2]$$

Figure 5-9 and Figure 5-10 report the iso-surface of reaction rate for the thermal way (R4) and the NNH way (R6). The volume in the thermal case is smaller than the NNH case in accord with the global production value.

The production from NNH starts very early, in the initial part of the flame in the duct, where the temperature is lower and where is the highest concentration of fuel and it evolves to around the high temperature zone.

The production from thermal way is located only where the temperature is over 2000K.

However the shape of these iso-surfaces indirectly confirms the diffusion aspect of the flame.

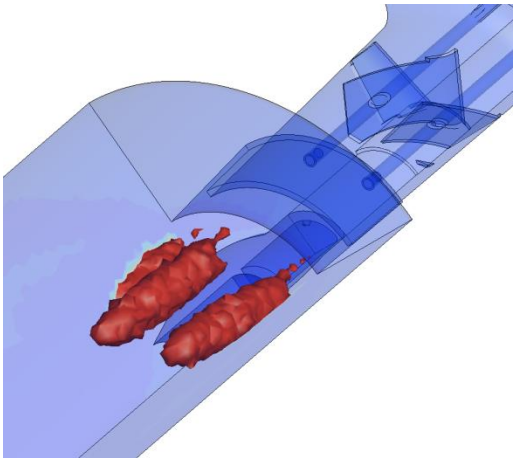

Figure 5-9 : Iso surface of rate NO thermal, value 10^{-5} kgmol/m^3s

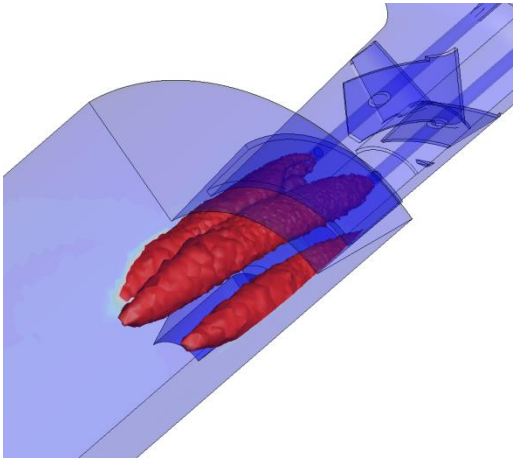

Figure 5-10 : Iso surface of rate NO via NNH, value 10^{-5} kgmol/m^3s

5.5 Operative pressure effect

All data from the examined case are in atmospheric pressure condition, but in a heavy duty gas turbine the pressure could be over 10 bar thus the influence on the NOx production could be important, as reported by Leonard et al. [54] and Biagioli et al. [55]. For this reason a new simulation campaign was performed where the investigated parameter was the operating pressure.

The simulations were performed in aerodynamics similitude, where the velocity was the same in all case and the thermal input was linear function of pressure. In this condition the flame shape could be similar between the cases.

The explored range was from 1 to 15 bar with 5 bar step, this is the typical range where the gas turbines are used for electric production operate, included the micro gas turbine.

Effect on Flame Shape

The first analysis is about the flame shape to verify that the theoretical similitude is correct, see Figure 5-11. Macroscopically there is a the similitude on the flame shape the main difference is the early ignition because the operative pressure increment delays it. The main change is for pressure over 10bar, in fact the Figure 5-12 reports the profile of C-premix rate near the fuel injection point. The lower cases, 1 and 5 bar, have the same profile but the 10 and 15 bar show a very low profile. Probably in this case the Reynolds number influence the ignition, in fact the Reynolds change from 10^3 to 10^5.

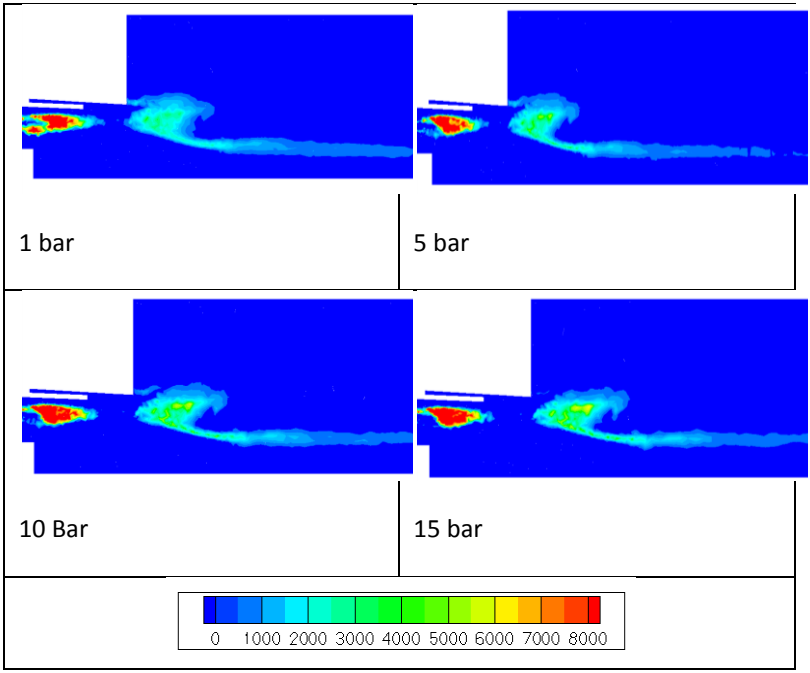

Figure 5-11: Premix - C rate at different operative pressure on a longitudinal plane

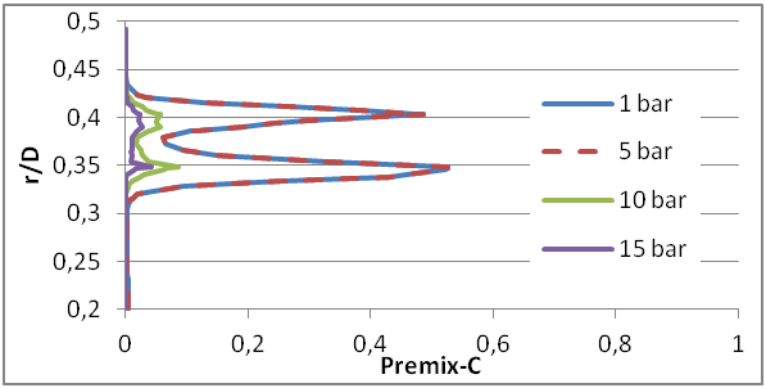

Figure 5-12: Premix - C rate profile near the fuel injection point at different operative pressure

Effect on NOx emission

The graph of Figure 5-13 reports the results of simulation using the decoupled post-processor, it shows a high total value for the NOx emissions.

The pattern shows a initial very high increment but over 10 bar there is a leveling. However the global value is lower with the reference case of diffusion flame system [40], 230 ppm vs 550 ppm.

About the production paths the result is similar than the atmospheric case where the main path isn't the thermal.

The analysis on Thermal NOx was performed with two postprocessor, the pure Zeldovich and the decoupled with a limited chemistry.

The Figure 5-14 reports the comparison, until a pressure of 10 bar the decoupled shows a lower value than the other but for the 15 bar pressure it presents a high increment.

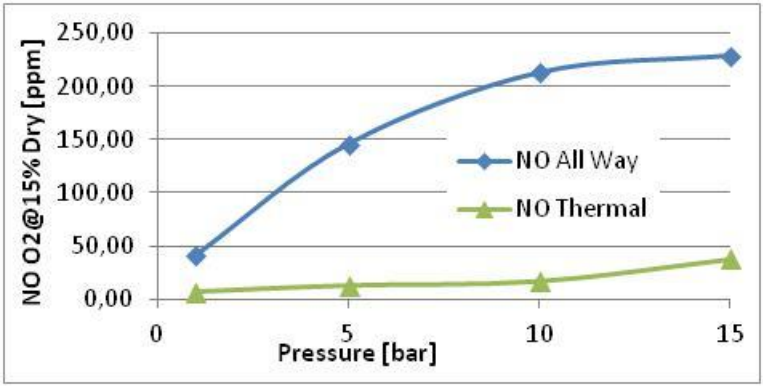

Figure 5-13: NOx evaluation against the operative pressure, all ways and thermal way

The pure Zeldovich works with a direct correlation where its inputs are the temperature and species fields, it doesn't consider the chemical interaction or other elements.

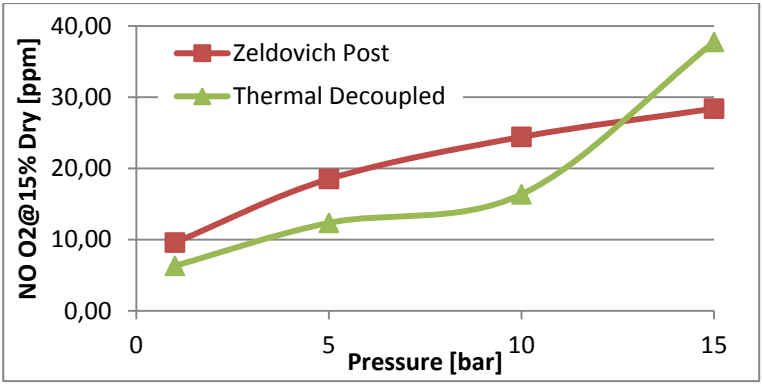

Figure 5-14: NOx evaluation against the operative pressure, Thermal way from Zeldovich postprocessor and Decoupled postprocessor

5.6 Conclusion

The update RANs modeling permit to integrate the information from the previous experimental analysis.

There are three new important information on the flame shape, the NOx emission path and the effect of operative pressure.

There is a early ignition but it isn't alike a flash back because there is a very stretched flame with a low temperature profile that doesn't involve the meal wall.

The NOx emissions in this flame are promoted by chemical paths as the NNH one instead the Zeldovich one.

The operative pressure influences a lot the NOx emission.

Chapter 6.

Design of MGT combustor

6.1 Intro

The results from the previous chapters show the limitations on the hydrogen fueling in gas turbine with the premix technology. Generally there is a early ignition, thus it needs a very high air flow, and the NOx emissions are very influenced by the operative pressure and by equivalence ratio.

A intent of this work is the identifying of the best application background for the hydrogen fueling in this contest the heavy duty machines are at a disadvantaged because the operative pressure and equivalent ratio are high.

However the micro gas turbines “MGTs” are a interesting class because the operative pressure is limited and the equivalence ratio is very low also Therkelsen et al. [14] obtained interesting result on a 60 kWel MGT.

The MGT is a regenerative gas turbine with a limited electric output, less than 100 kWel, used for distributed combined heat and power “CHP” system, [60,61]. This class is characterized by a very low NOx emission in natural gas fueling, less than 15 ppm @15% O2.

The emission regulation for this machines is more flexible than the big power plans thus it could be possible to operate with higher NOx emission.

In this chapter the analysis on a 100kWel MGT combustion chamber are reported to understand the capabilities of hydrogen fueling in this machine type.

6.2 Unit description

The analyzed combustion chamber is a reverse flow tubular combustor, natural gas fueled. The unit includes two swirler: the primary, for the pilot duct, the secondary works as premixing duct, [62].

The inner flame tube is the liner that contains the flame, while the outer flame tube drives the air to the swirlers, see Figure 6-1.

There are two different fuel lines: the pilot line (diffusive) and the main line (premixed).

In the primary zone there is the primary swirler and the nozzle of the pilot line that was coaxial with the combustion chamber, it's object is the stabilization of the flame from the main duct.

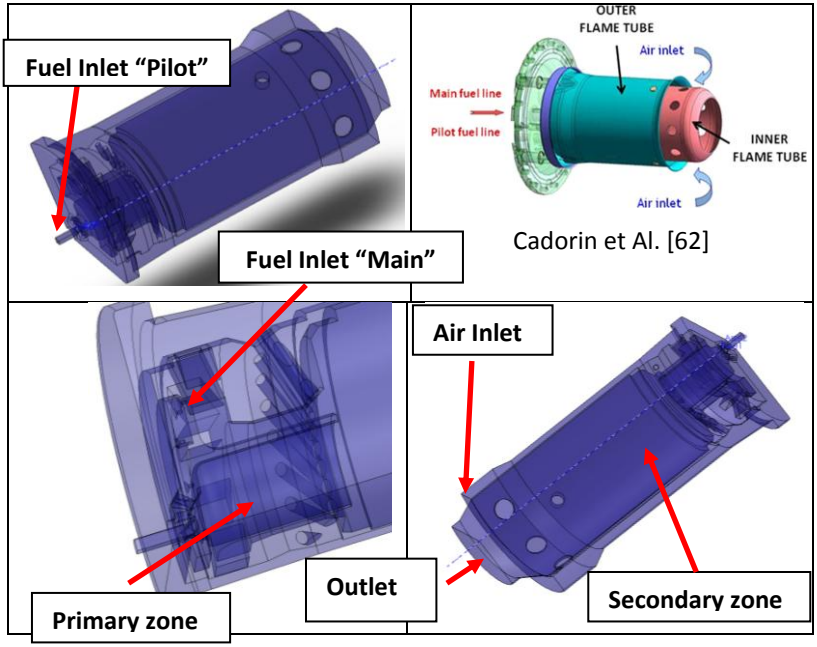

Figure 6-1: Combustor's images

The secondary swirler is radial type and the main fuel is introduced in this swirler by sixteen jet in cross injection. The obtained mixture flows into the secondary zone.

The air from the compressor enters the combustion chamber in counter-current compared to combustion gases, passing through the space between the outer and inner flame tubes.

The Table 6-1 and the Table 6-2 report the boundary condition for the full load operative point in Natural gas fueling.

Air		
Mass Flow	*kg/s*	0,7658
Temperature	*K*	871
Reference Press.	*Pa*	409.025

Table 6-1: Air boundary condition

Fuel		
Temperature	*K*	333
Main flow	*kg/s*	0,005942
Pilot flow	*kg/s*	0,001025
Total flow	*kg/s*	0,006967
Thermal Input	*kW*	348
Global equivalent ratio	-	0,13

Table 6-2: Fuel boundary condition

6.3 Numerical Simulation on original unit

The numerical simulation used to analyze the original MGT combustor is based on the same modeling setup of the last investigation on the premixer prototype, see Chapter 5. The investigated cases are the pure methane fueling and the pure hydrogen fueling.

The Figure 6-2 reports the axial velocity fields for the two cases, the hydrogen fueled presents a very different field respect the methane one. In the main flow, red circle, there is a high acceleration and it modifies all aerodynamics in the combustor. In the hydrogen case there is a high intensity depression, blue zone.

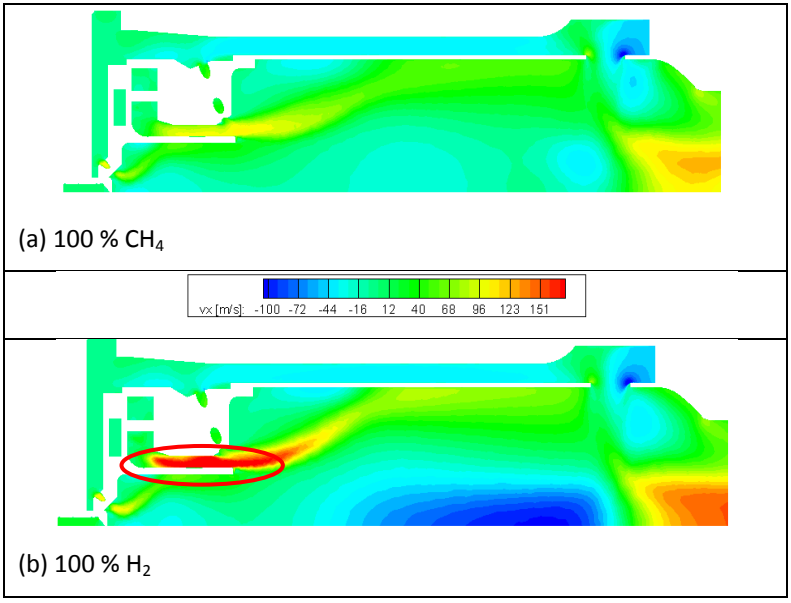

Figure 6-2: Axial Velocity fields on longitudinal plane.

The acceleration in the main flow for the hydrogen cases is caused by the early ignition of the fuel. In fact the Figure 6-3 reports a high temperature zone in the main duct for the hydrogen case, consequence of a flame.

The ignition is caused by the jet in cross that produces too turbulence, in fact this configuration was eliminated in the prototype of previous chapters. Also the shape of mixing duct doesn't permit to protect the metal wall by the flame thus for the hydrogen fueling a new design is needed.

The high depression in the secondary zone is caused by this early flame that was opener than the methane case.

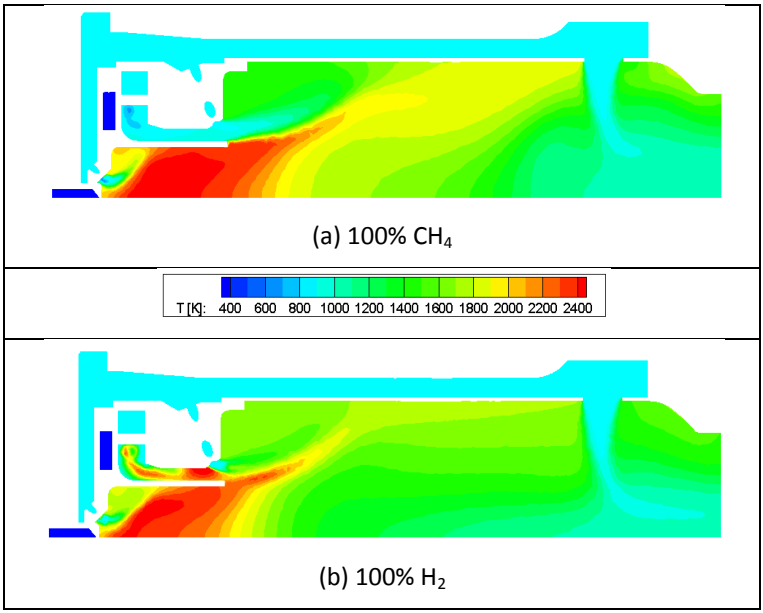

(a) 100% CH_4

(b) 100% H_2

Figure 6-3: Temperature fields on longitudinal plane.

6.4 Design of new combustor

The preliminary analysis proves how a natural gas design isn't adequate for hydrogen fueling in a gas turbine therefore the unit needs to be re-design. From the previous experience the new design is focus on the injection system and the premixing duct, see Figure 6-4.

The original primary zone is changed in the premixing duct and the radial swirler flows directly in it; the pilot's component are moved in the secondary zone. The premixing duct is converging to increase the outlet velocity, target about 120 m/s, and a air slot is added to cold the outlet edge.

A series of holes are added to permit a improvement of the cooling in the secondary zone.

The injection holes are placed on the back wall where was the original pilot. The hole configuration is eight in circle and one on the center, coaxial with the combustor, to place the flame on the combustor axis, far away from the metal wall, see Figure 6-5. The fuel injection velocity is about 170 m/s.

The first development roles is the mixing driving to a low turbulence system because in hydrogen fueling the turbulence causes the early ignition, this effect is obtained by the injection's direction and low difference of velocity between the air and the fuel. However the injection velocity has to be enough high to push away the flame.

The second development driver is on the position of injection point, the arrangement is defined to take advantage of the early ignition because it could be used to suffocate a fuel share.

The air distribution in the combustion chamber is changed to increase the flow in the primary zone, to reduce the equivalence ratio, by the modification of all air passages in the unit, see Table 6-3.

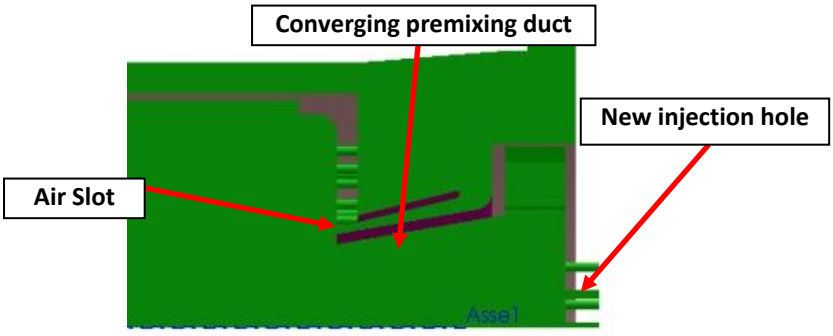

Figure 6-4: Re-designed combustor view on a longitudinal plane

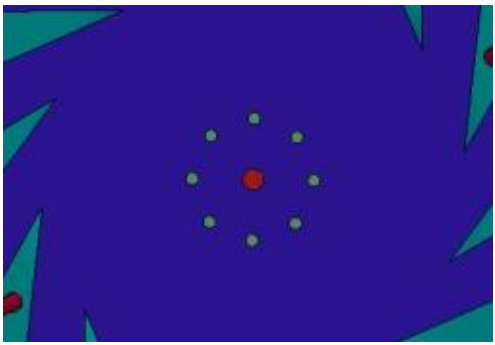

Figure 6-5: Injection system 8 +1 holes

	Equivalent ratio
Primary zone	0,252
Secondary zone	0,200
Global	0,130

Table 6-3: Equivalent ratio in the new combustor

6.5 CFD Analysis

A numerical simulation on the re-designed unit is performed to understand how the modifications are effective on the flame ant its interaction with the unit.

The aerodynamic in the combustion chamber, see Figure 6-6, is like than the previous prototype, in fact at the premix outlet there is a re-circulation zone caused by the swirled flow. In the original layout the swirler efficiency is limited by the duct shape. The increment of velocity in the premixing duct causes the increment of pressure drop on the combustion chamber to 6%, the original was less than 3%.

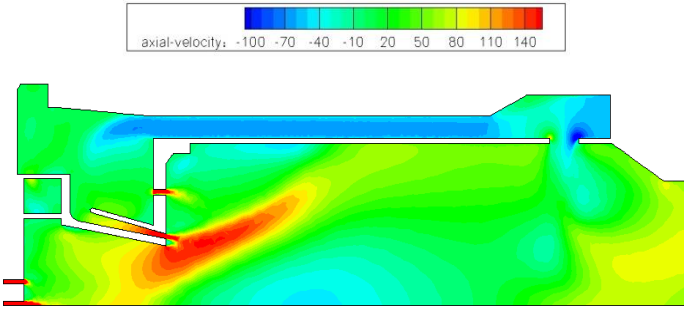

Figure 6-6: Axial Velocity field on longitudinal plane.

Also in this case there is a early ignition very close to the injection point, see Figure 6-7. In this units the injection is near a wall thus the air flow velocity is slow, it is limits of the radial layout for the swirler. The flame front presents a conical shape and it purses the main flow.

The temperature field is generally low, in fact there isn't zone with a temperature over 2000K, this is result of a good mixing.

The air flow is able to place the flame on the combustor axis in this way it is able protect the premixing duct's walls from the high temperature. About the NOx emission the total value is 82 ppm @15% O2, the thermal way is only 4 ppm @15% O2. In this case the not thermal way are more important than the prototype. Therkelsen et al. [63] obtained similar results with experimental campaign on H2 fueled 60kWel MGT.

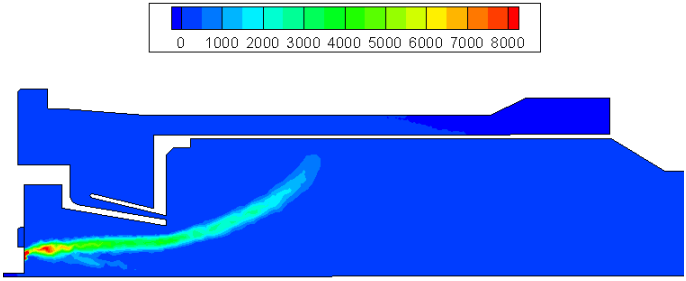

Figure 6-7: Premix rate field on longitudinal plane.

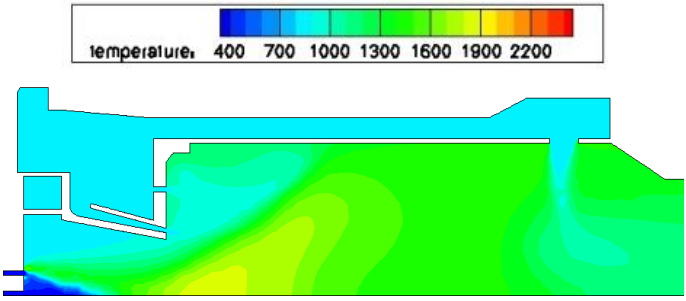

Figure 6-8: Temperature field on longitudinal plane.

	ppm @ 15% O2
All ways	82
Thermal way	4

Table 6-4: Evaluated NOx emissions

6.6 Final observation

This chapter reported the numerical analysis on a MGT combustion chamber, based on the numerical set-up defined in the previous chapter.

The original configuration isn't able to operate in pure hydrogen fueling than a new design is proposed to control the flame.

Also in this case the numerical simulation shows a early ignition probably only the using of a ceramic coated material permits a safe operating.

The NOx emission are quite high, 82 ppm, but for a MGT application could be acceptable because the regulation is more flexible.

Conclusions

The principal aim of the work on this thesis is the study of premixing technology in pure hydrogen fueled gas turbine.

The work is based on the design of a prototype and its analysis by experimental activity and numerical tools, only the union of this approaches is able to deal with exhaustively this complex topic.

The first result is the insufficiency of systems designed for natural gas when they are fueled with hydrogen, the flow velocity isn't enough and the mixing is based on too high turbulence. In this contest the high flame velocity of hydrogen causes the flash back. Also the tools, used for the natural gas analyzing, are limited for hydrogen flames. The NOx emission measured in a atmospheric test rig could be a undervaluation of actual value and the difference could be too big. The impossibility to see the complete flame could be a deficit. The numerical tools had to be improved because more details on chemistry and mixing are needed.

The premixing in hydrogen fueling is very difficult there is a early ignition that endangers the outcome. The flame is alike a stretched diffusion flame however the temperature field is as low as in a natural gas premixed system.

The obtained low temperature field is inefficacy to limit the NOx emission because the hydrogen fueling promotes path different than the thermal mechanism. The main interesting path is the NNH that works in the zone where the flame shows the early ignition, low temperature and high elementary H concentration.

In this NOx emission paths the effect of operative pressure on their production is very important and it could be a limits for the heavy duty gas turbines.

In this contest the micro gas turbine could be the application niche for the hydrogen fueling because they work with low operative pressure

and very low equivalence ratio thus they permit a better control on NOx emission, also the regulation is more flexible for this machines.

Also the components for adapting to hydrogen fueling, see ATEX normative, could be cheaper than for a heavy duty machine.

The development of a hydrogen fueled gas turbine combustor needs to be driven on a different way than the natural gas fueling. The first role is the reducing of the turbulence in the mixing zone and the second is using of the early ignition to suffocate a share of the fuel to delay the flame.

Acknowledgements

I would like to express my gratitude to my Tutor Prof. Francesco Martelli and Eng PhD Giovanni Riccio.

I'm also grateful to Stefano Sigali, Iarno Brunetti and all ENEL staff for their support in this work.

At least but not at last my collegues and friends of department "S. Stecco", Simone Salvadori, Alessandro Marini, Adriano Spadi, Matteo Prussi, Massimiliano Insinna, Robero Mussi, Andrea Rizzo, Alessandro Mattana, Leonardo Nibbi, David Chiaramonti and Simonetta Tegliai.

References

[1] CORREA S. M., 1993, “A Review of NOx Formation Under Gas-Turbine Combustion Conditions,” Combustion Science and Technology, **87**(1-6), pp. 329–362.

[2] Glassman I., 1996, Combustion, Academic press.

[3] Shelil N., Griffiths A., Bagdanavicius A., and Syred N., 2010, “Flashback Limits of Premixed H2/CH4 Flames in a Swirl-Stabilized Combustor,” Volume 2: Combustion, Fuels and Emissions, Parts A and B, ASME, pp. 1247–1258.

[4] Kwon O. C., and Faeth G. M., 2001, “Flame/stretch interactions of premixed hydrogen-fueled flames: measurements and predictions,” Combustion and Flame, **124**(4), pp. 590–610.

[5] Rozenchan G., Zhu D. L., Law C. K., and Tse S. D., 2002, “Outward propagation, burning velocities, and chemical effects of methane flames up to 60 ATM,” Proceedings of the Combustion Institute, **29**(2), pp. 1461–1470.

[6] Pareja J., Burbano H. J., Amell A., and Carvajal J., 2011, “Laminar burning velocities and flame stability analysis of hydrogen/air premixed flames at low pressure,” International Journal of Hydrogen Energy, **36**(10), pp. 6317–6324.

[7] KITAGAWA T., NAKAHARA T., MARUYAMA K., KADO K., HAYAKAWA A., and KOBAYASHI S., 2008, “Turbulent burning velocity of hydrogen–air premixed propagating flames at elevated pressures,” International Journal of Hydrogen Energy, **33**(20), pp. 5842–5849.

[8] Hu E., Huang Z., He J., Miao H., and Zheng J., 2009, “Experimental and numerical study on laminar burning velocities and

flame instabilities of hydrogen–air mixtures at elevated pressures and temperatures," International Journal of Hydrogen Energy, **34**(13), pp. 5574–5584.

[9] Verhelst S., T'Joen C., Vancoillie J., and Demuynck J., 2011, "A correlation for the laminar burning velocity for use in hydrogen spark ignition engine simulation," International Journal of Hydrogen Energy, **36**(1), pp. 957–974.

[10] DURBIN M. D., and BALLAL D. R., "Studies of lean blowout in a step swirl combustor," Journal of engineering for gas turbines and power, **118**(1), pp. 72–77.

[11] Schefer R. W., 2003, "Hydrogen enrichment for improved lean flame stability," International Journal of Hydrogen Energy, **28**(10), pp. 1131–1141.

[12] Noble D. R., Zhang Q., Shareef A., Tootle J., Meyers A., and Lieuwen T., 2006, "SYNGAS MIXTURE COMPOSITION EFFECTS UPON FLASHBACK AND BLOWOUT," ASME Turbo Expo 2006: Power for Land, Sea and Air.

[13] Lieuwen T., McDonell V., Petersen E., and Santavicca D., 2006, "Fuel Flexibility Influences on Premixed Combustor Blowout, Flashback, Autoignition and Instability," Volume 1: Combustion and Fuels, Education, ASME, pp. 601–615.

[14] Therkelsen P., Mauzey J., McDonell V. G., and Samuelsen S., 2006, "Evaluation of a Low Emission Gas Turbine Operated on Hydrogen," ASME Turbo Expo 2006: Power for Land, Sea and Air, Asme, pp. 557–564.

[15] Marek C., and Smith T., 2005, “Low emission hydrogen combustors for gas turbines using lean direct injection,” 41 st AIAA/ASME/SAE/ASEE Joint, pp. 1–27.

[16] Hsu A. T., Anand M. S., and Razdan M. K., 1996, “‘An Assessment of PDF Versus Finite-Volume Methods for Turbulent Reacting Flow Calculations,” AIAA paper AIAA-96-0523.

[17] James S., Anand M. S., Razdan M. K., and Pope S. B., 2001, “In Situ Detailed Chemistry Calculations in Combustor Flow Analyses,” Journal of Engineering for Gas Turbines and Power, **123**(4), p. 747.

[18] Pope S. B., 1997, “Computationally efficient implementation of combustion chemistry using in situ adaptive tabulation,” Combustion Theory and Modelling, **1**(1), pp. 41–63.

[19] Bilger R. W., 1993, “Conditional moment closure for turbulent reacting flow,” Physics of Fluids A: Fluid Dynamics, **5**(2), p. 436.

[20] Brewster B. S., Cannon S. M., Farmer J. R., and Meng F., 1999, “Modeling of lean premixed combustion in stationary gas turbines,” Progress in Energy and Combustion Science, **25**, pp. 353–385.

[21] Zimont V., Polifke W., Bettelini M., and Weisenstein W., 1998, “An Efficient Computational Model for Premixed Turbulent Combustion at High Reynolds Numbers Based on a Turbulent Flame Speed Closure,” Journal of Engineering for Gas Turbines and Power, **120**(3), p. 526.

[22] Zimont V. L., 2000, “Gas premixed combustion at high turbulence. Turbulent flame closure combustion model,” Experimental Thermal and Fluid Science, **21**(1-3), pp. 179–186.

[23] Peters N., and Rogg B., 1992, “Reduced kinetic mechanisms for applications in combustion systems,” Lecture Notes in Physics Monographs, **15**.

[24] Campelo M. H., Muppalat S. P. R., Wen J. X., and Manickam B., 2010, “NUMERICAL INVESTIGATION OF LAMINAR BURNING VELOCITIES FOR VARIOUS PREMIXED GASEOUS HYDROGEN/HYDROCARBON/AIR MIXTURES,” ECCOMAS 2010.

[25] Ströhle J., and Myhrvold T., 2007, “An evaluation of detailed reaction mechanisms for hydrogen combustion under gas turbine conditions,” International Journal of Hydrogen Energy, **32**(1), pp. 125–135.

[26] Göttgens J., Mauss F., and Peters N., 1992, “Analytic approximations of burning velocities and flame thicknesses of lean hydrogen, methane, ethylene, ethane, acetylene, and propane flames,” Symposium (International) on Combustion, **24**(1), pp. 129–135.

[27] Marini A., Cappelletti A., Riccio G., and Martelli F., 2010, “Cfd re-design of a gas turbine can-type combustion chamber hydrogen fired,” ECCOMAS CFD 2010, June 14-17, Lisbon, Portugal.

[28] Riccio G., Marini A., and Martelli F., 2009, “Numerical investigations of gas turbine combustion chamber Hydrogen fired,” ISABE-2009-1112.

[29] Cappelletti A., 2009, “Analisi di sistemi per la combustione premiscelata ad h2,” Università degli Studi di Firenze.

[30] Burmberger S., Hirsch C., and Sattelmayer T., 2006, “Designing a Radial Swirler Vortex Breakdown Burner.”

[31] Lilley D. G., 1986, “Swirling flows in typical combustor geometries,” Journal of Propulsion and Power, **2**(1), pp. 64–72.

[32] Tiribuzi S., 2004, “CFD Modelling of Thermoacoustic Oscillations Inside an Atmospheric Test Rig Generated by a DLN Burner,” ASME Conference Proceedings, ASME, pp. 475–485.

[33] Kaskan W. E., 1957, “The dependence of flame temperature on mass burning velocity,” Symposium (International) on Combustion, Elsevier, pp. 134–143.

[34] Ballester J., and García-Armingol T., 2010, “Diagnostic techniques for the monitoring and control of practical flames,” Progress in Energy and Combustion Science, **36**(4), pp. 375–411.

[35] Guethe F., Guyot D., Singla G., Noiray N., and Schuermans B., 2012, “Chemiluminescence as diagnostic tool in the development of gas turbines,” Applied Physics B, **107**(3), pp. 619–636.

[36] Guyot D., Guethe F., Schuermans B., Lacarelle A., and Paschereit C. O., 2010, “CH*/OH* Chemiluminescence Response of an Atmospheric Premixed Flame Under Varying Operating Conditions,” ASME Turbo Expo 2010: Power for Land, Sea, and Air (GT2010), **2**, pp. 933–944.

[37] Luckerath R., Lammel O., Stohr M., Boxx I., Stopper U., Meier W., Janus B., and Wegner B., 2011, “Experimental Investigations of Flame Stabilization of a Gas Turbine Combustor,” ASME Conference Proceedings, **2011**(54624), pp. 725–736.

[38] Kaskan W. E., 1959, “Abnormal Excitation of OH in H2/O2/N2 Flames,” The Journal of Chemical Physics, **31**(4), p. 944.

[39] Kathrotia T., Fikri M., Bozkurt M., Hartmann M., Riedel U., and Schulz C., 2010, “Study of the H+O+M reaction forming OH*: Kinetics of OH* chemiluminescence in hydrogen combustion systems,” Combustion and Flame, **157**(7), pp. 1261–1273.

[40] Brunetti I., Rossi N., Sigali S., Sonato G., and Cocchi S., 2010, “ENEL’s Fusina zero emission combined cycle: experiencing hydrogen combustion,” POWERGEN EUROPE.

[41] ANSYS, 2012, “ANSYS FLUENT Theory Guide.”

[42] Schluter J., Pitsch H., Moin P., Shankaran S., Kim S., and Alonso J., 2003, “Towards Multi-Component Analysis of Gas Turbines by CFD: Integration of RANS and LES Flow Solvers,” ASME Conference Proceedings, **2003**(36843), pp. 101–109.

[43] Boudier G., Gicquel L. Y. M., Poinsot T. J., Bissières D., and Bérat C., 2007, “Comparison of LES, RANS and experiments in an aeronautical gas turbine combustion chamber,” Proceedings of the Combustion Institute, **31**(2), pp. 3075–3082.

[44] Moureau V., Domingo P., and Vervisch L., 2010, “STUDYING SWIRLING FLAMES USING HIGHLY RESOLVED SIMULATIONS OF AN INDUSTRIAL PREMIXED BURNER,” ECCOMAS 2010, Lisbona, pp. 14–17.

[45] Fröhlich J., and Von Terzi D., 2008, “Hybrid LES/RANS methods for the simulation of turbulent flows,” Progress in Aerospace Sciences, **44**(5), pp. 349–377.

[46] Menter F. R., and Egorov Y., 2005, “A scale adaptive simulation model using two-equation models,” AIAA, **1095**(1095), p. 2005.

[47] Abou-Taouk A., and Eriksson L.-E., 2011, “Optimized Global Mechanisms for CFD Analysis of Swirl-Stabilized Syngas Burner for Gas Turbines,” ASME 2011 Turbo Expo: Turbine Technical Conference and Exposition (GT2011), ASME, pp. 765–779.

[48] Menter F. R., and Egorov Y., 2006, “SAS Turbulence Modelling of Technical Flows,” Direct and Large-Eddy Simulation, **VI**, pp. 687–694.

[49] Menter F. R., and Egorov Y., 2010, “The Scale-Adaptive Simulation Method for Unsteady Turbulent Flow Predictions. Part 1: Theory and Model Description,” Flow Turbulence and Combustion, **85**(1), pp. 113–138.

[50] Rotta J., 1972, Turbulente Stromungen., Published by B. G. Teubner.

[51] Menter F. R., 1994, "Two-equation eddy-viscosity turbulence models for engineering applications," AIAA journal, **32**(8), pp. 1598–1605.

[52] Bozzelli J. W., and Dean A. M., 1995, "O + NNH: A possible new route for NOX formation in flames," International Journal of Chemical Kinetics, **27**(11), pp. 1097–1109.

[53] Skottene M., and Rian K. E., 2007, "A study of NOx formation in hydrogen flames," International Journal of Hydrogen Energy, **32**(15), pp. 3572–3585.

[54] Leonard G., and Stegmaier J., 1994, "Development of an Aeroderivative Gas Turbine Dry Low Emissions Combustion System," Journal of Engineering for Gas Turbines and Power, **116**(3), p. 542.

[55] Biagioli F., and Güthe F., 2007, "Effect of pressure and fuel–air unmixedness on NOx emissions from industrial gas turbine burners," Combustion and Flame, **151**(1-2), pp. 274–288.

[56] Smith G. P., Golden D. M., Frenklach M., Moriarty N. W., Eiteneer B., Goldenber M., Bowman C. T., Hanso R. K., Song S., William C. Gardiner J., Lissianski V. V., and Qin Z., "GRI-MECH 3.0," p. http://www.me.berkeley.edu/gri_mech/.

[57] Li J., Zhao Z., Kazakov A., and Dryer F. L., 2004, "An updated comprehensive kinetic model of hydrogen combustion," Int. J. Chem. Kinet, **36**, pp. 566–575.

[58] Centaursoft, "Centaur," p. http://www.centaursoft.com/.

[59] MILLER J., BRANCH M., and KEE R., 1981, “A chemical kinetic model for the selective reduction of nitric oxide by ammonia,” Combustion and Flame, **43**, pp. 81–98.

[60] Pilavachi P. A., 2002, “Mini- and micro-gas turbines for combined heat and power,” Applied Thermal Engineering, **22**(18), pp. 2003–2014.

[61] Hamilton S., 2003, The Handbook of Microturbine Generators, PennWell Books.

[62] Cadorin M., Pinelli M., Vaccari A., Calabria R., Chiariello F., Massoli P., and Bianchi E., 2012, “Analysis of a Micro Gas Turbine Fed by Natural Gas and Synthesis Gas: MGT Test Bench and Combustor CFD Analysis,” Journal of Engineering for Gas Turbines and Power, **134**(7), p. 071401.

[63] Therkelsen P., Werts T., McDonell V. G., and Samuelsen S., 2009, “Analysis of NO[sub x] Formation in a Hydrogen-Fueled Gas Turbine Engine,” Journal of Engineering for Gas Turbines and Power, **131**(3), p. 031507.

Images Index